Int. J. Mech. Sci. Vol. 25, No. 5, pp. 305–335, 1983
Printed in Great Britain.

0020–7403/83/050305–31$03.00/0
Pergamon Press Ltd.

A VISCOUS SHELL FORMULATION FOR THE ANALYSIS OF THIN SHEET METAL FORMING

E. OÑATE
E. T. S. Ing. de Caminos, Univ. Politécnica de Barcelona, Barcelona, Spain

and

O. C. ZIENKIEWICZ
Civil Engineering Dept. University College of Swansea, Swansea, Wales

(*Received* 13 *November* 1981; *in revised form* 21 *August* 1982)

Summary—A finite element method to analyse large plastic deformations of thin sheets of metal is presented. The formulation is based on an extension of the general viscoplastic flow theory for continuum problems to deal with thin shells. Axisymmetric situations are considered first and here the simple two noded reduced integration element is used. Numerical results for the stretch forming and deep drawing of circular sheets are presented and comparison with experimental results is made. The second part of the paper deals with the deformation of sheets of arbitrary shape. The general viscous shell element is derived from the standard reduced integration, "thick shell element. Numerical results for simple 3-D sheet forming problems are given.

NOTATION

$\epsilon_{ij}, \dot{\epsilon}_{ij}$	strain and strain rate tensors
σ_{ij}	stress tensor
Γ_{ijkl}	non linear constitutive tensor
C_{ijkl}	elasticity constitutive tensor
T	temperature
μ	viscosity
p	pressure
G	shear modulus
$\hat{U}_i, U_i$	displacement, velocity
γ	fluidity parameter
n	power coefficient in viscoplastic law
$\bar{\epsilon}, \dot{\bar{\epsilon}}$	strain and strain rate invariants
σ_y	uniaxial yield stress
$\mathbf{K}$	stiffness matrix
$\mathbf{a}$	nodal displacements vector
$\mathbf{f}$	nodal forces vector
ϵ	convergence error norm
$t, \Delta t$	time and time increment
$\epsilon_r, \epsilon_\theta$ ($\dot{\epsilon}_r, \dot{\epsilon}_\theta$)	membrane strain (membrane strain rate)
K_s, K_θ ($\dot{K}_s, \dot{K}_\theta$)	flexural strain (flexural strain rate)
γ, ($\dot{\gamma}$)	shear strain (shear strain rate)
$\epsilon_t, \dot{\epsilon}_t$	thickness strain (thickness strain rate)
$\mathbf{S}$	strain transformation matrix
$\mathbf{D}, \hat{\mathbf{D}}, \mathbf{D}_1, \mathbf{D}_2$	elasticity matrices
ν	Poisson's ratio
$\mathbf{L}$	strain operator
r, z	radial and vertical coordinates
$\mathbf{b}, \mathbf{t}, \mathbf{p}$	body forces, surface loads and point loads vectors
A	transverse area
N_i	shape function for node i
ξ, η, ζ	local coordinates for the element
$\mathbf{B}$	strain matrix
ϕ	element angle with z-axis
h	element thickness
$\mathbf{T}$	displacements transformation matrix
β, γ, α	friction coordinate system angles
$\bar{\sigma}$	stress invariant
R_p, V_p	punch radius and punch velocity
$\bar{\mu}$	Coulomb friction coefficient
α_i, β_i	nodal normal rotations
$\mathbf{J}$	Jacobian matrix
$\boldsymbol{\theta}$	orthogonal transformation matrix for strains
R	normal anisotropy parameter
l	linear element length

1. INTRODUCTION

Stamping of sheet metal parts by means of punches and dies is a standard manufacturing process. However, despite its broad application in industry, the design of forming processes is largely based on experimental techniques, such as the use of circular grid systems [1, 2] or forging limit diagrams [3–6].

The development of reliable analytical procedures to predict the behaviour of sheet metal deformation processes has encountered many serious obstacles. Together with the non linearity of the material properties other important effects like the unsteady nature of the process, the large magnitudes of the stains involved and the importance of the friction effects at the tool-sheet interface [7–12], make the study of stamping processes so complex that its analysis leads to large scale computer requirements.

Axisymmetric stamping processes are obviously easier to treat than the more general problem. Nevertheless, the complexity of the mechanics of this problem is still considerable, and it has been the subject of comprehensive analyses by many researchers. Experimental results have been reported by Lankford *et al.* [13] Whitely [14] and Hecker [5] amongst many others [15–19]. Numerical results using the Levy–Mises theory of plasticity for isotropic materials were reported by Chung and Swift [16] and Woo [17–19]. Extensions of the Levy–Mises equations to deal with transversal anisotropy effects using the incremental theory of plasticity have been used by Wang [21], Kagtanoglu and Alexander [22] and Moore and Wallace [23]. Elastoplastic solutions have been reported by Chang and Kobayashi [24], Wifii [25], Yamada [26–27], Gotoh [28] and Wang and Budianski [29] Fukui *et al.* analysed deep drawing problems using a total strain theory [30]. Elasto-viscoplastic and rigid-plastic solutions have been obtained respectively by Wang and Wenner [15] and Kobayshi and Kim [15]. A comprehensive account of the subject can be found in Ref. [31].

This procedure, commonly known as the "flow approach" was introduced originally by Goon *et al.* [33] and it has been extensively used with success by many [34–42] to deal with two dimensional and axisymmetric metal forming processes.

The first attempt to use the flow formulation to study the large plastic deformation of sheets of metal was reported by Zienkiewicz *et al.* [32] who used the general three dimensional continuum formulation to analyse axisymmetric deep drawing and stretch forming problems. However, full three dimensional solutions of sheet metal stamping problems using the flow approach are expensive and when sheets are formed some simplifications can be introduced. These follow a simple adaptation of thin shell theory to the flow approach to give what has been termed a a "viscous shell" formulation.

This approach has already been presented by the authors and numerical results showing the applicability of the method to axisymmetric stamping processes were proved to be successful [43–46].

The object of this paper is to present in a comprehensive form the basis of the viscous shell formulation for axisymmetric and general 3D stamping problems.

The formulation allows for strain hardening phenomena, friction effects and treatment of anistropy. Techniques for dealing with these problems are also given in detail.

Many stamping processes in industry are axisymmetric, e.g. the forming of cups by deep drawing or pure stretching of circular blanks using hemispherical or flat bottom punches. Therefore, in this paper special attention has been focussed on the axisymmetric formulation of the viscous shell approach which is presented first, together with numerical examples of its application to stretch forming and deep drawing problems. However, the general procedure allows the treatment of the deformation of thin sheets of irregular shape as such as occur in the motor car industry and in the second part of the paper a 3-D viscous shell formulation which can deal with those problems is presented. Naturally conputational difficulties for such a general case are large and solutions costly.

In the next section some basic background material is given.

2. BASIC THEORY AND CONSTITUTIVE RELATIONS FOR A VON MISES TYPE FLOW

If elastic deformations are neglected, a general description of behaviour of most materials can be given in terms of viscoplasticity with the strain rates defined by a relationship of the form

$$\dot{\epsilon}_{ij} = \Gamma_{ijkl}\sigma_{kl} \tag{1}$$

where

$$\Gamma = \Gamma(\sigma_{ij}, T, \dot{\epsilon}_{ij}) \tag{2}$$

is a symmetric tensor. The full formulation can be found in Ref. [47a, b] as well as in Ref. [32].† If we compare equation (1) with the standard elasticity form

$$\epsilon_{ij} = C_{ijkl}\sigma_{kl} \tag{3}$$

we can see immediately that there is one to one correspondence between the viscoplastic flow equations and those of an equivalent *quasistatic elastic* problem if we interchange the variables of velocity by displacement, strain by strain rate and the elasticity constitutive matrix by the non linear flow constitutive matrix

For a von Mises type of Perzyna's plastic or viscoplastic material, as is the case with metals and many other materials [47], the form of matrix Γ can be easily obtained [32]. *This implies incompressible behaviour of the material* and thus the analogous elastic problem must satisfy the incompressibility requirements.

The equations which express the above analogy can then be written in a compact form as:

Viscoplastic flow — *Incompressible elasticity*

Equilibrium

$$\sigma_{ij,j} + b_i = 0. \tag{4}$$

Stress/strain rate relationship — *Stress/strain relationship*

$$\dot{\epsilon}_{ij} = \frac{1}{2\mu}(\sigma_{ij} - \delta_{ij}p) \qquad \epsilon_{ij} = \frac{1}{2G}(\sigma_{ij} - \delta_{ij}p). \tag{5}$$

Strain rate — *Strain*

$$\dot{\epsilon}_{ij} = \frac{1}{2}(u_{i,j} + u_{j,i}) \qquad \epsilon_{ij} = \frac{1}{2}(\hat{u}_{i,j} + \hat{u}_{j,i}). \tag{6}$$

Velocity: u_i — *Displacement*: $\hat{u}_i$.

In above, p is the mean normal stress, δ_{ij} the Dirac delta, G the shear modulus which plays a role analogous to the non linear viscosity, μ, which in the flow problem is given by [32]‡

$$\mu = \frac{\sigma_y + (\dot{\bar{\epsilon}}/\gamma)^{1/n}}{3\dot{\bar{\epsilon}}}. \tag{7}$$

In above σ_y is the uniaxial yield stress of the material, γ and n are physical parameters of the viscoplasticity model used and $\dot{\bar{\epsilon}}$ is a strain rate invariant defined as

$$\dot{\bar{\epsilon}} = \sqrt{\left(\frac{2}{3}\dot{\epsilon}_{ij}\right)\epsilon_{ij}}. \tag{8}$$

For pure plasticity $\gamma \to \infty$ and equation (7) yields simply

$$\mu = \frac{\sigma_y}{3\dot{\bar{\epsilon}}}. \tag{9}$$

The analogy between viscoplastic flow/incompressible elasticity shown in eqs. (4)–(6) allows the treatment of pure plastic–viscoplastic flow problems using computer programs developed for linear elasticity, and simply allowing the elastic constant G to be a function of the stress or strain level [32].

A point should be mentioned here. The basis of the above analogy requires that incompressibility conditions must be satisfied in both the viscoplastic and elastic solutions. For a Von Mises type of

†An appendix is included in this paper for completeness. In this some of the expressions of the section are derived in detail.

‡Note: In Ref. [32] the value of μ is obtained as $\mu: \dfrac{\left(\sigma_y + \left[\dfrac{\dot{\bar{\epsilon}}}{\sqrt{3}\gamma}\right]^{1/n}\right)}{\sqrt{3}\,\dot{\bar{\epsilon}}}$. The difference with that of equation (7) is due to the definition of $\dot{\bar{\epsilon}}$ which in Ref. [32] is defined as $\sqrt{(2\dot{\epsilon}_{ij}\dot{\epsilon}_{ij})}$.

Perzyna's viscoplastic material incompressible behaviour is implicit (i.e. $\dot{\epsilon}_{ii} = 0$). However, in the computational solution the incompressibility constraint must be deliberately imposed. This can be done in various ways which range from the use of Lagrange multipliers, to the use of the simple penalty forms. All these procedures have been extensively tested and used to analyse plane and axisymmetric metal forming continuum problems [32, 34–36, 42].

The viscoplastic flow/elasticity analogy described in this section is the basis for the viscous shell formulation which follows an identical pattern. This is described in the next section.

3. THE VISCOUS SHELL APPROACH

The viscoplastic flow/elasticity analogy procedure described in the previous section can obviously be used for three dimensional situations such as shells and the main difficulty is the size of the problem which makes the cost of the solution, expensive.

Shell theory is a simplification of 3D elasticity when one of the dimensions of the problem is small compared with the rest. If the creeping flow formulation is simplified in the same way, there exists an identical analogy between the simplified form of the incompressible creeping flow equations using the shell theory assumptions, (hereafter this will be referred to as the "viscous shell formulation") and that for incompressible elastic shell theory. *This analogy allows the immediate treatment of large plastic deformations of thin sheets of metal as incompressible elastic shell problems*, and direct use can be made of shell theory just replacing, as in the continuum solution, displacements by velocities, strains by their rates and the shear modulus by the shell viscosity which remains a function of the stress or strain level.

One of the main advantages of this analogy is that, since plane stress assumptions are implicit in shell theory, the incompressibility constraint now presents no difficulty and incompressible behaviour can be easily achieved by simply adjusting the shell thickness as the solution progreses to ensure constant volume.

Sheet metal deformation are problems for which steady state conditions do not exist and the problem has to be analysed as a transient one. The velocity of the flow is first established for the initial configuration and then these velocities, determined at a boundary node, allow the new position of the boundary to be determined after a time increment, Δt, by a suitable updating procedure. With the new boundary and now an altered mesh, new flow conditions are established, and the general process can then be restated.

As each flow solution starts determining the velocity component in the current configuration very large deformations can be readily followed by a simple process of repetition of the solution in updated coordinates. The solution scheme thus follows

(1) Identify an incompressible shell elastic solution. If standard finite element techniques are used, a discrete system of equations is obtained upon discretisation, of the form [52]

$$\mathbf{K}\mathbf{a} = \mathbf{f} \tag{10}$$

where $\mathbf{K}$ is the shell stiffness matrix, $\mathbf{a}$ and $\mathbf{f}$ are the nodal displacement and nodal forces vectors respectively. The equivalent viscous shell is formulated simply identifying displacements and strains with velocities and strain rates respectively and the shear modulus with the non linear viscosity.

Equation (10) becomes a system of *non linear equations* which must be solved iteratively. In the analysis incompressibility is obtained by simply putting the Poissons ratio $\nu = 0.5$.

(2) In the initial configuration, assume some initial value of the velocities, $\mathbf{a}^0$, or extrapolate these from previous configurations.

(3) Using appropriate strain rate expressions, μ_0 is found from equation (7) or (9) and $\mathbf{K}_0 = \mathbf{K}_0(\mathbf{a}^0)$ is computed.

(4) Solve for $\mathbf{a}^1$. If direct iteration is used the first iteration becomes,

$$\mathbf{a}^1 = \mathbf{K}_0^{-1}\mathbf{f}. \tag{11}$$

(5) Check for convergence. If desired convergence is not achieved go back to 3 and start the process with the new velocity field obtained. Convergence implies satisfaction of an error norm. We have chosen

$$\frac{\Sigma(a_i^n - a_i^{n-1})^2}{\Sigma(a_i^n)^2} \leqslant \epsilon^2 \tag{12}$$

Here ϵ equal to 0·01 has been used.

(6) Once convergence has been achieved update geometry by $\mathbf{a}\Delta t$ where Δt is an appropriate time step size, and change boundary conditions if new points have come into contact with the tool surface. Also update the sheet thickness using the incompressibility condition.

(7) Start the process again extrapolating from the velocity field previously obtained.

3.1 *Strain hardening effects*

The change of yield strength with the deformation process is easily included in the calculation and, indeed, very little additional cost is involved. Neglecting temperature effects and assuming the yield strength σ_y independent of the mean stress, p, we can express this, as a function of the strain and strain-rate only as

$$\sigma_y = f(\dot{\bar{\epsilon}}, \bar{\epsilon}). \tag{13}$$

As at each stage of the deformation the strain rates and the second strain rate invariant, $\dot{\bar{\epsilon}}$ are known. The total (scalar) effective second strain invariant, $\bar{\epsilon}$ can simply be evaluated from

$$\bar{\epsilon}^{t+\Delta t} = \bar{\epsilon}^t + \int_t^{t+\Delta t} \dot{\bar{\epsilon}} \Delta t \tag{14}$$

and the yield stress appropriately updated.

3.2 *Treatment of friction*

The algorithm used to simulate friction effects between the tool-sheet interface is more complex than for continuum problems where non-directional friction laws can be simply introduced[32]. In most sheet metal deformation problems the tool comes progressively into contact with the sheet as the deformation increases and the slippage directions between tool and blank change accordingly. In the algorithm used in this paper at the end of each iteration the reactions at each contact node in a "friction coordinate system", i.e. in directions along a tangent plane common to all elements adjacent to the node, are checked. If the value of the forces in the tangential directions, contained in such a plane, exceeds the value of the normal force times a friction coefficient, the node is allowed to slip in the appropriate tangential direction and a prescribed friction force is applied at the node. The normal velocity of the node is then constrained to the value of the normal velocity of the punch if the node is in contact with the punch (or to zero if the node is in contact with a fixed point of the tool.

4. AXISYMMETRIC VISCOUS SHELL FORMULATION

Axisymmetric forming processes are obviously easier to treat than the more general problem. Nevertheless, the complexity of the mechanics of this problem is still considerable and it has been the subject of comprehensive analysis by many researchers.

In this section we will show that the viscous shell approach can be used effectively to deal with axisymmetric sheet metal forming problems. The basis of the success of the method lies in the efficiency of the analogous elastic shell solution. The finite element shell formulation used here is the one presented by Zienkiewicz *et al.*[48]. The success of such a formulation lies in its simplicity (straight elements are used) and its versatility to treat both thick and thin axisymmetric shell type problems.

4.1 *Background theory*

In a general curvilinear system the "generalized strains" in an axisymmetric shell (under axisymmetric load), see Fig. 1, can be written following action in Ref. [48] as:

$$\begin{Bmatrix} \epsilon_r^0 \\ \epsilon_\theta^0 \\ K_s \\ K_\theta \\ \gamma^0 \end{Bmatrix} = \begin{Bmatrix} \dfrac{du'}{ds} + \dfrac{v'}{R} \\ (v' \cos\phi + u' \sin\phi)/r \\ -\dfrac{d\beta}{ds} + \dfrac{d}{ds}(v'/R) \\ -\sin\phi \left(\beta - \dfrac{u}{R}\right)/r \\ \dfrac{dv'}{ds} - \beta \end{Bmatrix} = \mathbf{L}\hat{\mathbf{u}} \tag{15}$$

with

$$\mathbf{L} = \begin{bmatrix} \dfrac{d}{ds}, & \dfrac{1}{R}, & 0 \\ \dfrac{\sin\phi}{r}, & \dfrac{\cos\phi}{r}, & 0 \\ 0, & \dfrac{d}{ds}\left(\dfrac{1}{R}\right), & -\dfrac{d}{ds} \\ \dfrac{\sin\phi}{rR}, & 0, & -\dfrac{\sin\phi}{r} \\ 0, & \dfrac{d}{ds}, & -1 \end{bmatrix}$$

$$\hat{\mathbf{u}} = \begin{Bmatrix} u' \\ v' \\ \beta \end{Bmatrix} \tag{16}$$

where ϵ_r^0 and ϵ_θ^0 correspond to membrane strains, K_s and K_θ to flexural strains, γ^0 is the shear strain and u', v' and β are the tangential and normal displacements and the normal rotation respectively of a point in the middle surface of the shell (see Fig. 1).

Actual strains at any point can be simply obtained from generalised strains assuming that plane sections remain plane, by

$$\boldsymbol{\epsilon} = \begin{Bmatrix} \epsilon_r \\ \epsilon_\theta \\ \gamma \end{Bmatrix} = \begin{Bmatrix} \epsilon_r^0 + zK_s \\ \epsilon_\theta^0 + zK_\theta \\ \gamma^0 \end{Bmatrix} = \mathbf{S}\boldsymbol{\epsilon}^0 \tag{17}$$

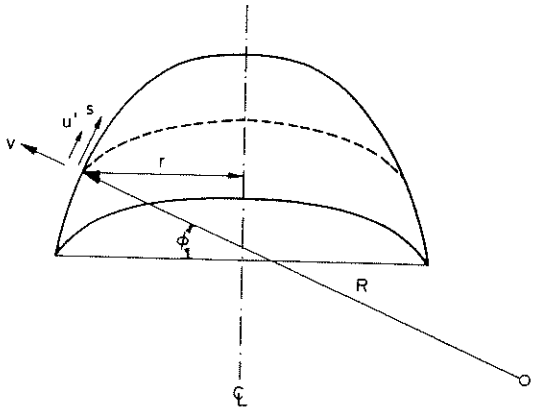

FIG. 1. Axisymmetric shell defination.

with

$$\mathbf{S} = \begin{bmatrix} 1 & 0 & z & 0 & 0 \\ 0 & 1 & 0 & z & 0 \\ 0 & 0 & 0 & 0 & 1 \end{bmatrix} \tag{18}$$

where z is the coordinate in the thickness direction. As previously mentioned, the incompressibility condition is easily satisfied solving for ϵ_z and making

$$\epsilon_z = -(\epsilon_r + \epsilon_\theta). \tag{19}$$

Therefore at each stage of the deformation the thickness can be modified according to the current thickness strain to ensure constant volume.

Stresses are then related with actual strains in a standard manner by

$$\boldsymbol{\sigma} = \begin{Bmatrix} \sigma_r \\ \sigma_\theta \\ \tau \end{Bmatrix} = \hat{\mathbf{D}}\boldsymbol{\epsilon} \tag{20}$$

where $\hat{\mathbf{D}}$ is the elasticity matrix which for *incompressible materials* (Poisson's ratio $\nu = 0.5$) is given by [48]

$$\hat{\mathbf{D}} = G \begin{Bmatrix} 4 & 2 & 0 \\ 2 & 4 & 0 \\ 0 & 0 & 1 \end{Bmatrix} = G\mathbf{D}^0 \tag{21}$$

where G is the shear modulus. If use is now made of the elastic/viscous shell analogy previously mentioned, the basic viscous shell expressions analogous to equations (15), (20) and (21) are directly obtained as

$$\dot{\boldsymbol{\epsilon}}^0 = \mathbf{L}\mathbf{u} \quad \text{(strain rate-displacement)} \tag{22}$$

$$\boldsymbol{\sigma} = \hat{\mathbf{D}}\dot{\boldsymbol{\epsilon}} \quad \text{(constitutive relation)} \tag{23}$$

$$\hat{\mathbf{D}} = \mu\mathbf{D}^0 \tag{24}$$

where $\mathbf{u}$ and $\dot{\boldsymbol{\epsilon}}$ are respectively the velocity and the strain rate vectors of a point in the middle surface of the "viscous shell" and μ is the non linear viscosity defined in equation (7), which for pure plastic flow can be obtained as

$$\mu = \frac{\sigma_y}{3\sqrt{(4\dot{\epsilon}^2 + 4\dot{\epsilon}_\theta^2 + 4\epsilon_r\epsilon_\theta + \gamma^2)}} \tag{25}$$

The virtual work equation of the system can be written as

$$\int_s \int_0^4 \delta\boldsymbol{\epsilon}^T \boldsymbol{\sigma} 2\pi r \, ds \, dt = E.W. \tag{26}$$

where

$$E.W. = \int_s \delta\mathbf{u}^T \mathbf{b} 2\pi r h \, ds + \int_s \delta\mathbf{u}^T \mathbf{t} 2\pi r \, ds + 2\pi r \delta\mathbf{u}^T \mathbf{p} \tag{27}$$

is the external work done by the body forces, $\mathbf{b}$, surface loads, $\bar{\mathbf{t}}$ and line loads, $\mathbf{p}$, and h is the shell thickness.

Using equations (17) and (20) the virtual work equation of the ystem, e.g. (26), can be written as

$$2n \int\int (\boldsymbol{\epsilon}^0)^T \mathbf{D} \boldsymbol{\epsilon}^0 r \, dr \, dz = E.W. \tag{28}$$

where

$$\mathbf{D} = \mathbf{S}^T \hat{\mathbf{D}} \mathbf{S} = \mu \left[\begin{array}{cccc|c} 4 & 2 & 4z & 2z & 0 \\ 2 & 4 & 2z & 4z & 0 \\ 4z & 2z & 4z^2 & 2z^2 & 0 \\ 2z & 4z & 2z^2 & 4z^2 & 0 \\ \hline 0 & 0 & 0 & 0 & 1 \end{array}\right] = \begin{bmatrix} \mathbf{D}^{mf} & \mathbf{0} \\ \mathbf{0} & \mathbf{D}^s \end{bmatrix} \tag{29}$$

is the equivalent elasticity matrix which is now a function of the non-linear viscosity.

Equation (28) is the basis for the finite element discretisation which is described in the next section.

4.2 *Finite element discretisation: linear element*

With the above formulation we note immediately that a finite element interpolation involving only C^0 continuity [48] is required as only first derivatives of u', v' and p occur. Obviously any of the numerous isoparametric finite element formulations are possible [52].

With an interpolation of the type

$$\mathbf{u}' = \begin{Bmatrix} u' \\ v' \\ \beta \end{Bmatrix} = \Sigma N_i q_i'; \quad \mathbf{e}_i' = \begin{Bmatrix} m_i' \\ v_i' \\ p_i \end{Bmatrix} \tag{30}$$

the form of the discretized equations can be obtainded in a fairly straight-forward manner [48, 52].

4.3 *Linear element*

For a straight element, as that of Fig. 2 the simplest interpolation can be written as

$$\mathbf{N}_i = N_i \mathbf{I} \text{ with } \quad N_i = (1 + \eta\eta_i)/1; \quad \eta = \frac{2s}{l}; \quad \eta_i = \frac{2s_i}{l} \tag{31}$$

in above l is the element length with nodes at $\eta = \pm 1$.

The strain vector can be easily expressed in terms of the element nodal variables a_i' as

$$\boldsymbol{\epsilon}^0 = \Sigma \mathbf{B}_i \mathbf{a}_i' \tag{32}$$

where $\mathbf{B}_i$ is the strain matrix of node i obtained from Eq. (15) putting $R = \infty$ as the element is straight, viz:

$$\mathbf{B}_i = \left[\begin{array}{ccc} \dfrac{dN_c}{ds} & 0 & 0 \\ N_i \dfrac{\sin\phi}{r} & N_i \dfrac{\cos\phi}{r} & 0 \\ 0 & 0 & -\dfrac{dN_i}{ds} \\ 0 & 0 & -N_i \dfrac{\sin\phi}{r} \\ \hline 0 & \dfrac{dN_c}{ds} & -N_i \end{array}\right] = \begin{bmatrix} \mathbf{B}_i^{mf} \\ \mathbf{B}_i^s \end{bmatrix}. \tag{33}$$

Equation (32) can be used directly to obtain the discretized system of equations upon substitution in the virtual work expression equation (28). Standard manipulations give the element matrices as

$$\mathbf{K}_{ij}^{e'} = n \int_{-1}^{1} \int_{-h/2}^{h/2} [\mathbf{B}_i^{mf}]^T \mathbf{D}^{mf} \mathbf{B}_j^{mf} r l \, d\eta \, dz + n \int_{-1}^{1} \int_{-h/2}^{h/2} [\mathbf{B}_i^s]^T \mathbf{D}^s \mathbf{B}_j^s \mathbf{B}_j^s r l \, d\eta \, dz \tag{34}$$

$$= \mathbf{K}_{ij}^{mf} + \mathbf{K}_{ij}^s$$

$$\mathbf{f}_i^e = n \int_{-1}^{1} \mathbf{N}_i \mathbf{b} r l h \, d\eta + n \int_{-1}^{1} \mathbf{N}_i \bar{\mathbf{t}} r l \, d\eta + 2n r_i \mathbf{p}_i \tag{35}$$

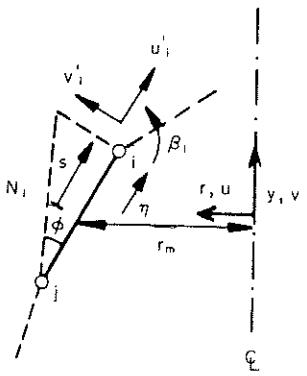

FIG. 2. Linear element.

where $\mathbf{K}_{ij}^{e}$ is the element local stiffness matrix connecting two nodes ij and $\mathbf{f}_i$ is the nodal local forces vector of node i.

Due to the strain dependence of the **D** matrix, integration across the thickness must be performed numerically. In the cup forming problems presented in this paper, in zones where the bending strain rates are small in comparison with the membrane strain rates a three point Simpson's integration rule has proved to be sufficient. On the other hand, in zones where plastic bending is significant a five point Simpson's rule has been used. The stiffness matrix **K** can be formed assembling the individual stiffness matrices.

As elements meeting at a node can have different directions it is necessary to transform the stiffness matrices so that at each common node the nodal displacements and forces are expressed in a common and uniquely defined global coordinate system.

The element stiffness matrix $\mathbf{K}^e$ in the global cartesian system (ry) (see Fig. 2) is given by standard expression

$$\mathbf{K}_{ij}^{e} = \mathbf{T}^T \mathbf{K}_{ij}^{e'} \mathbf{T} \tag{36}$$

where **T** is the transformation matrix for the element which relates local displacements or forces with those in the cartesian system and it is given by

$$\mathbf{T} = \begin{bmatrix} -\sin\phi & \cos\phi & 0 \\ \cos\phi & \sin\phi & 0 \\ 0 & 0 & 1 \end{bmatrix} \tag{37}$$

where ϕ is the element angle identified in Fig. 2. The stiffness equation in the global system can thus be written after assembely as

$$\mathbf{K}\mathbf{a} = \mathbf{f}. \tag{38}$$

In above, all the matrices and vectors are expressed in the cartesian system. A further important point should be mentioned here. When the thickness of the shell is very small, the terms of matrix $\mathbf{K}_{ij}^{s}$ in equation (34) become much larger than those of matrix $\mathbf{K}_{ij}^{mf}$ and tend to overconstrain the numerical solution[48]. To overcome this problem, a "reduced integration technique" must be used, i.e. the terms of matrix $\mathbf{K}_{ij}^{s}$ are numerically integrated with a Gaussian quadrature order less than the order needed for its exact integration. We will not go here in the details of such a technique which can be found in many Refs. [48–53]. For practical purposes we will just state that $\mathbf{K}_{ij}^{s}$ matrix is integrated with a one point Gaussian quadrature rule in the s direction. The remainder of the stiffness matrix, can be evaluated exactly using a two point rule, *but accurate results are obtained if a single point is used for all calculations.* Clearly an explicit form of the element matrices can be written now by simply replacing the integrals in equation (34) by the appropriate values of the integral evaluated at the element mid-point. ($\eta = 0$, $r = r_m$).

4.4 *Treatment of friction*

Friction effects between tools and blank interfaces are taken into account in the analysis following the lines explained previously viz. Fig. 3. However, some simplifications can be introduced due to the symmetry of the problem.

It has been assumed that a node in contact with the tool will slip along a direction which is taken as the average of the directions of the elements adjacent to that node ($\bar{u}$ direction in Fig. 4). Therefore, at each node the stiffness matrices are assembled in a "friction cordinate system", defined by the direction of displacements $\bar{u}$ and $\bar{v}$ in Fig. 5, which automatically gives the forces in those directions, and allows checking of the slipping conditions at the node as previously explained (see Fig. 3). Standard manipulations lead to the stiffness equation in the friction coordinate system for the element as:

$$\bar{\mathbf{K}}^e = \bar{\mathbf{f}}^e \tag{39}$$

where $\bar{\mathbf{a}}^e$ and $\bar{\mathbf{f}}^e$ are the nodal displacement and nodal force vector in the friction system and $\bar{\mathbf{K}}^e$ is the element stiffness matrix in the local friction system defined at each node.

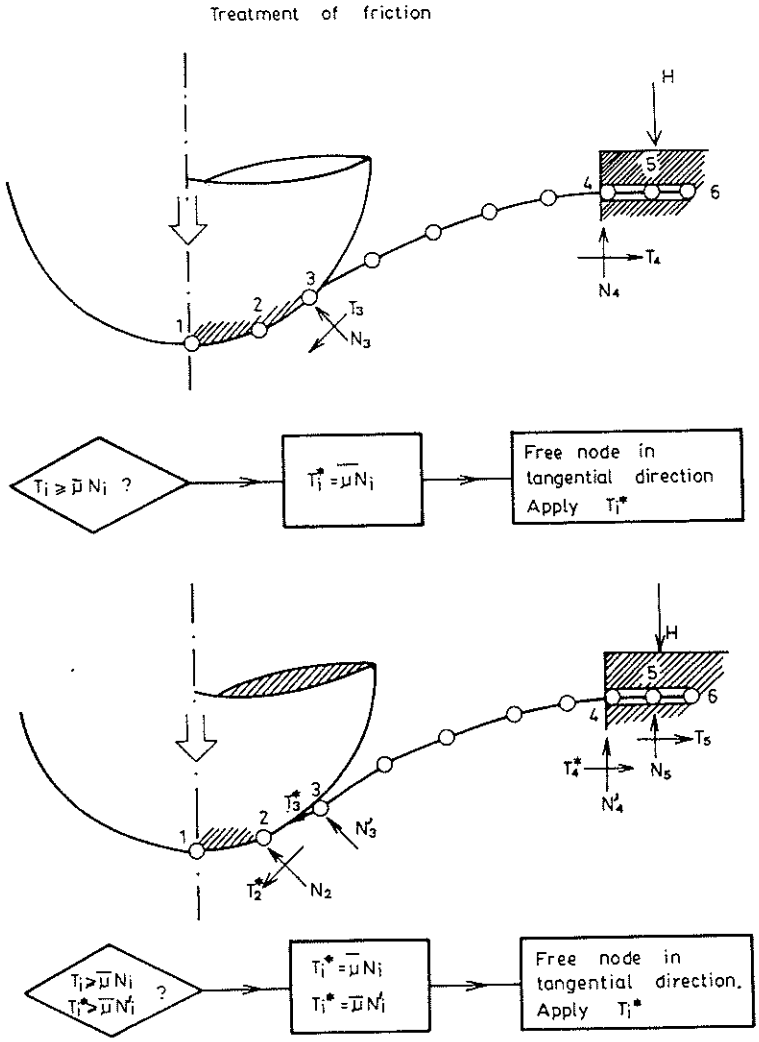

FIG. 3. Treatment of friction.

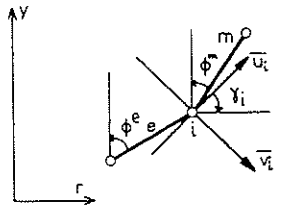

FIG. 4. Punch and blank geometry at an intermediate stage.

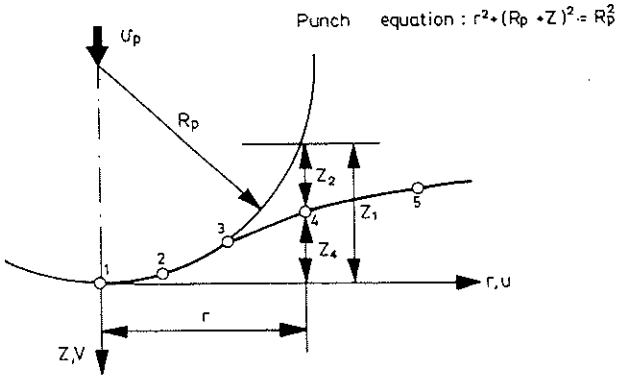

FIG. 5. Friction coordinate axes.

Now

$$\bar{\mathbf{K}}'^{e}_{ij} = \mathbf{F}_i^T \mathbf{K}'^{e} \mathbf{F}_j \tag{40}$$

with

$$\mathbf{F}_i = \begin{bmatrix} \sin\beta_i^- & -\cos\beta_i^- & 0 \\ \cos\beta_i^- & \sin\beta_i^- & 0 \\ 0 & 0 & 1 \end{bmatrix} \tag{41}$$

$$\beta_i^- = \frac{n}{2} \mp \frac{1}{2}(\phi^e + \phi_i^m). \tag{42}$$

(ϕ_i^m is the angle of the next element and ϕ is the angle which the element e forms with the vertical axis (as on Fig. 2). Assembly of the element matrices follows the standard process (52).

Finally, it is worth noting that the time increment calculation and geometry updating are both performed in the global cartesian system. Thus, once the solution has converged in the friction system, displacements and forces are transformed into their cartesian nodal components **a** and **f** respectively by

$$\mathbf{a}_i = \mathbf{F}_i \bar{\mathbf{a}}_i \tag{43}$$

$$\mathbf{f}_i = \mathbf{F}_i \mathbf{f}'_i \tag{44}$$

4.5 *Treatment of normal anisotropy*

If the material is anisotropic, the axisymmetric solution is no larger valid and a full three dimensional analysis taking into account the change of direction of the principal axes of anistropy must be carried out. However, it is usual to assume that the sheet exhibits the same properties in all directions in its plane but its properties in the perpendicular direction, i.e., through the thickness, are different. This type of anisotropy, termed "normal anisotropy" can be *very easily* included in the viscous shell formulation presented earlier simply noting that in the evaluation of the element stiffness matrix, integration through the thickness is performed numerically (see equation 34). *This allows the modelling of a non uniform material property distribution through the thickness by taking a different value of the viscosity, μ of equation* (25) *at each integration point in the thickness direction.* Accuracy of the process will obviously depend on the number of integration points we take to represent a given variation of properties through the thickness.

Frequently such normal anisotropy effects are simply characterised by a coefficient of anisotropy, R, defined as

$$R = \frac{\epsilon_\theta}{\epsilon_z}. \tag{45}$$

This is assumed to remain constant during the straining process and allows modelling of anisotropy in the thickness direction in a simple manner. This procedure has been used by some to assess the effects of normal anisotropy in the deformation of thin sheets of metal. It can be shown [54, 55], that for pure plastic flow this simply implies the replacement of matrix $\hat{\mathbf{D}}$ of equation (24) with a new matrix defined in terms of R by

$$\hat{\mathbf{D}} = \frac{\bar{\sigma}}{3\dot{\bar{\epsilon}}} \begin{bmatrix} \frac{2(2+R)(1+R)}{1+2R} & \frac{2(2+R)R}{1+2R} & 0 \\ \frac{2(2+R)+R}{1+2R} & \frac{2(2+R)(1+R)}{1+2R} & 0 \\ 0 & 0 & \frac{2+R}{1+2R} \end{bmatrix} \tag{46}$$

here $\bar{\sigma}$ and $\dot{\bar{\epsilon}}$ are respectively the equivalent yield stress and the effective strain rate for a material with such normally anisotropic properties. It can be shown that for axisymmetric situations [54]

$$\bar{\sigma} = \sqrt{\left(\frac{3(1+R)}{2(2+R)}\left\{\sigma_r^2 + \sigma_\theta^2 + \frac{2R}{1+R}\,\sigma_r\sigma_\theta + 2\frac{(1+2R)}{1+R}\,\tau_{r\theta}^2\right\}\right)} \tag{47}$$

$$\dot{\bar{\epsilon}} = \sqrt{\left(\frac{2(1+R)(2+R)}{3(1+2R)}\left\{\dot{\epsilon}_r^2 + \dot{\epsilon}_\theta^2 + \left(\frac{2R}{1+R}\right)\dot{\epsilon}_r\dot{\epsilon}_0 + \frac{1}{2(1+R)}\,\dot{\gamma}_{r\theta}^2\right\}\right)}. \tag{48}$$

Matrix **D** used for the numerical computation of stiffness matrix can be obtained by equation (29).

4.6 *Increment computation and geometry updating*

Thin sheet metal forming processes are moving boundary problems, i.e. the shape of the new boundary has to be updated every time convergence of the velocity field is achieved, and the limit of the blank/tool contact surface subsequently adjusted. This involves a time step computation which will be described.

We will be concerned here with the calculation of the time increment for which the first node of the

non-contacting region comes into contact with the indenting punch. An intermediate configuration at a time t_1 is shown in Fig. 5. Nodes 1, 2 and 3 are already in contact with the punch and node 4 is the first node in the non contacting region which will come into contact.

The equation of the punch in the coordinate axes, r, z of Fig. 4 is

$$r^2 + (R_p + z)^2 = R_p^2 \tag{49}$$

where R_p is the punch radius. If (r_4, z_4) and (u_4, v_4) are respectively the coordinates and velocities of nodal point 4 at time t_1, the new coordinates (r_4', z_4') at a time $t_1 + \Delta t_1$ will be

$$r_4' = r_4 + u_4 \Delta t_1$$

$$z_4' = z_4 + v_4 \Delta t_1 - v_4 \Delta t \tag{50}$$

where v_p is the punch velocity. From Fig. 5 we see that node 4 will come into contact when

$$z_4' = z_1 \tag{51}$$

The value of z_1 at time $t_1 + \Delta t$ is from equation (49)

$$-z_1' = \sqrt{(R_p^2 - r_4'^2)} - R_p. \tag{52}$$

Therefore, at time $t_1 + \Delta t_1$ node 4 will come into contact with the punch if

$$z_4 + (v_p - v_4)\Delta t_1 = \sqrt{(R_p^2 - (r_4 + u_4 \Delta t_1)^2} 2 - R_p \tag{53}$$

which is a non linear equation in Δt_1 which is determined by its solution. If a direct Euler iteration scheme is used we have for the nth iteration

$$\Delta t_1^n = \frac{z_1^{n-1} - z_4}{(v_p - v_4)}. \tag{54}$$

The process stops when the error norm, is less than a prescribed value. Here we have taken

$$\frac{\Delta t_1^n - \Delta t^{n-1}}{\Delta t_1^n} < 0.01. \tag{56}$$

Convergence of the above process has proved to be very fast and this has been used in all the examples shown in next section.

The simplest updating procedure is to use the time step calculated in equation (55) to increment the blank coordinates by $a\Delta t$ to its new deformed position so that we can be sure that the deformed blank does not cross the punch surface. However, the use of large time steps leads to instability and usually a small fraction of the time step calculated in equation (57) must be used [43, 46].

This is very necessary when a large portion of the blank has come into contact with the punch and the value of the time increment for the next free node to come into contact is big.

5. EXAMPLES

By using the finite element procedure described in proceeding sections numerical results have been obtained for the hemispherical stretching and deep drawing of circular isotropic ($R = 1$) thin sheets of metal.

Total strains at a time t have been calculated using the following

$$\epsilon_\theta^0 = \ln\left\{\frac{r^t}{r^0}\right\} \tag{56}$$

$$\epsilon_z^t = \epsilon_z^{t-\Delta t} + (\dot{\epsilon}_r^{t-\Delta t} + \dot{\epsilon}_\theta^{t-\Delta t})\Delta t \tag{57}$$

where r^t is the radius of a point at time t. The radial strain has been evaluated at the centre of the element by

$$e_r^t = \ln\left\{\frac{\text{length at time } t}{\text{initial length}}\right\} \tag{58}$$

and then extrapolated to the nodes by averaging the values of adjacent elements.

5.1 *Example* 1. *Hemispherical punch stretching*

The geometrical configuration of the problem and the stress/effective strain curve of the material can be seen in Fig. 6. The circular sheet of metal is restrained from moving horizontally and vertically at its edges but not from rotating.

To study the effect of friction between the blank/punch interface in the strain distributions, the problem has been analysed separately for five different friction coefficients of $= 0.0$, 0.04, 0.2, 0.5 and full friction, $\bar{\mu} = \infty$, respectively. Analytical and experimental results for this problem for $\mu = 0.04$ have been reported by Woo [19]. Fig. 6 shows the load/displacement curves for the various friction coefficients. We see that the

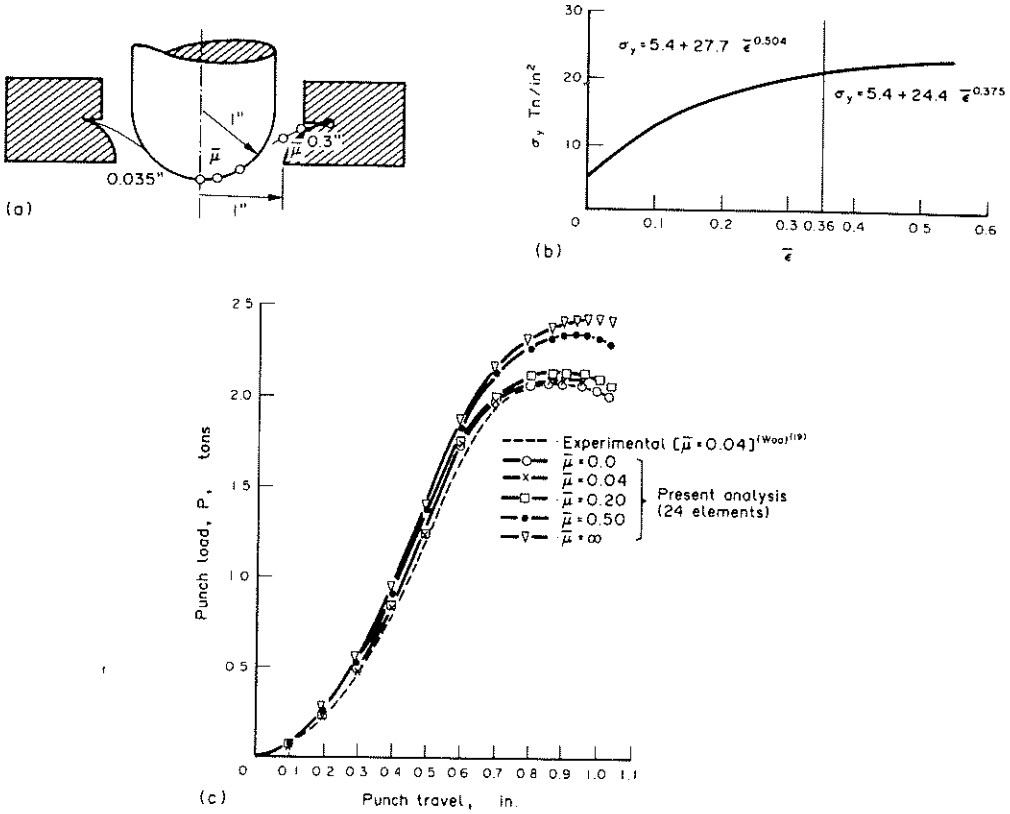

FIG. 6. Punch load-punch travel for various friction coefficients.

load/displacement curves are very similar for all friction coefficients except in the vicinity of the maximum load which increases slightly with higher friction. This phenomenon has been also reported by Kim *et al.*[56]. Numerical results for the circumferential and thickness strain distributions for a friction coefficient of 0.04 agree with the experimental values. We see that to get a uniform thinning of the sheet of metal, friction conditions should be dept as low as possible (Figs. 7 and 8), whereas an increase of the friction coefficient develops, as expected, a peak in the distribution of strain which moves outward with the deformation as it can be seen in Figs. 9–11.

The higher the value of the friction coefficient the more pronounced this peak becomes. The case of full friction, $\bar{\mu} = \infty$, in Fig. 11 is a clear example of a limiting situation when points in contact with the piston are restrained from moving radially (see strain paths) and the "crown" of thin material moves very rapidly towards the clamped edge.

Also in Fig. 8 the thinnest point of the sheet for the maximum load is indicated by an arrow. The radial position of such a point (for $\bar{\mu} = 0.04$) is 0.26" and agrees very closely with the experimental value of 0.25". This value coincided in the experiment with the fracture point (see Ref. [19]).

Figs. 12–17 show the deformed configuration of the sheet at different stages of the deformation for the various friction coefficients. Note the different final thickness distribution with low and high friction conditions.

5.2 *Example 2. Hemispherical deep drawing*

The problem is essentially similar to that described in last section but the edges of the sheet of metal are now free to move radially. The geometrical configuration of the problem is shown in Fig. 18. The stress/effective strain curve is as in the previous example (see Fig. 6).

Fig. 18 shows punch load/displacement curves for three different friction coefficients of $\bar{\mu} = 0.04$, $= 0.2$ and $= 0.5$ in punch/sheet interface. The coefficient of friction in the die region has been kept constant and equal to 0.04 for all cases. Again we notice that the maximum load increase slightly with higher friction.

The strain distribution for the three friction coefficients are shown in Figs. 19–21. The effect of friction is again noticeable and similarly, (but in not as pronounced a way as in the previous example), the thinnest point of the sheet moves radially towards the pole with decreasing friction. Results for $\bar{\mu} = 0.04$ agree well with experimental ones[18] (see Fig. 19) and show the severe thickness strain suffered by the material in the punch region. This strain is less pronounced when the friction coefficients between the surface of the sheet metal and the punch increase (see Figs. 20, 21). In a deep drawing operation friction is desirable in the punch region to lessen the straining over the punch head (as we can see in Figs. 20, 21), thereby improving the drawability of the material, since such straining may lead to local necking and instability. On the other hand, in an operation involving mainly stretch forming action, uniform straining of the material is necessary to give a deeper pressing. In such cases, friction should be kept as low as possible by effective lubrication.

The deformed geometry of the sheet at different stages of the deformation for the various friction

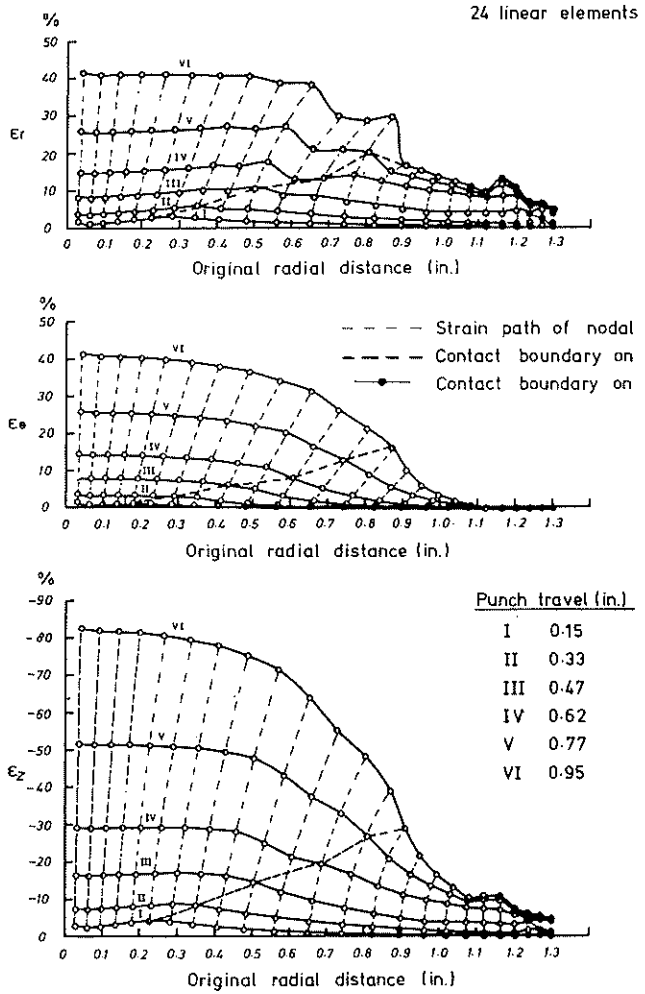

FIG. 7. Strain distributions for $\bar{\mu} = 0.0$.

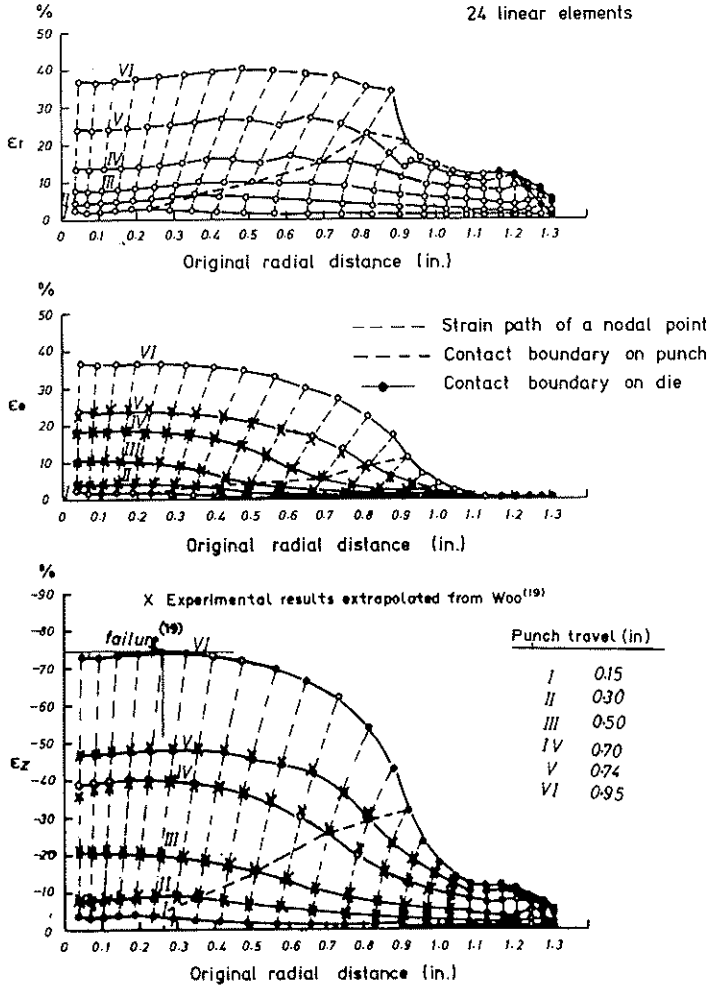

FIG. 8. Strain distributions for $\bar{\mu} = 0.04$.

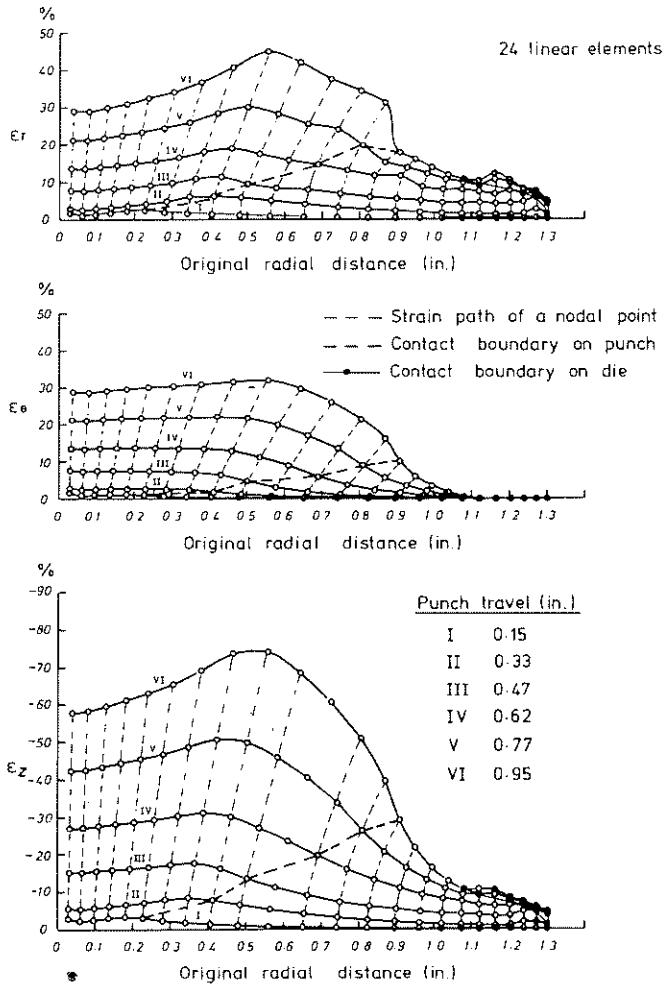

FIG. 9. Strain distributions for $\bar{\mu} = 0.20$.

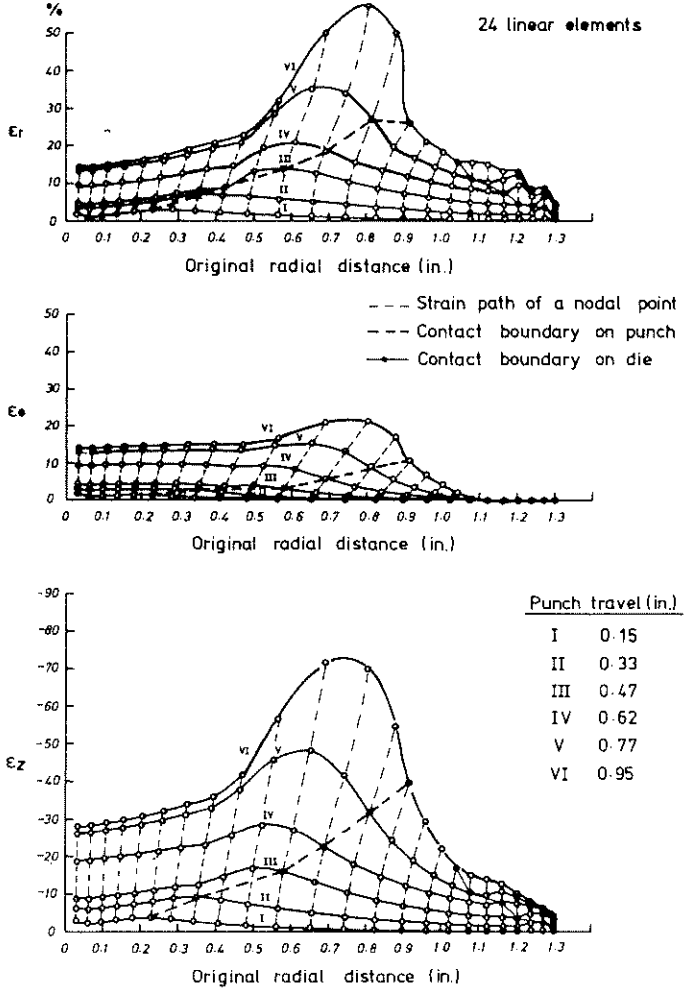

FIG. 10. Strain distributions for $\bar{\mu} = 0.50$.

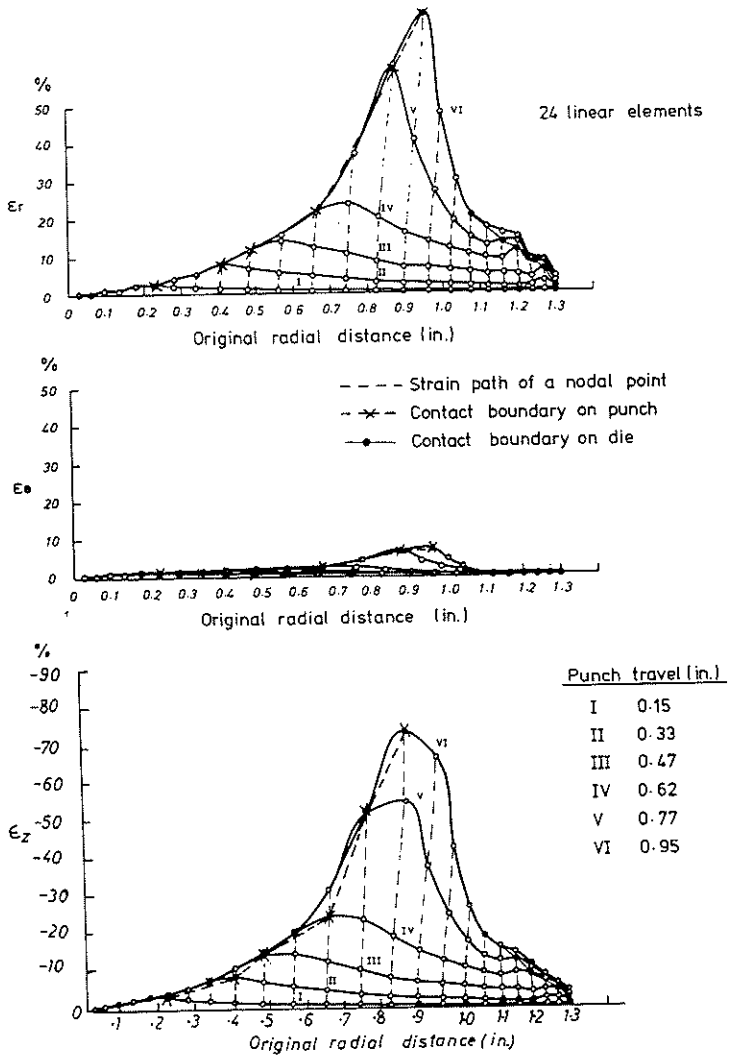

FIG. 11. Strain distributions for $\bar{\mu} = \infty$.

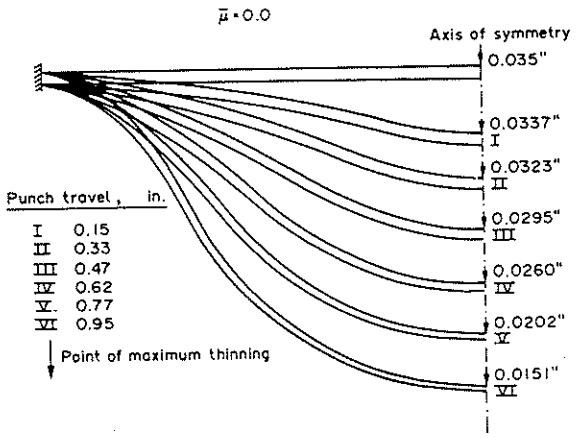

FIG. 12. Relative deformation of the sheet. 24 elements $\bar{\mu} = 0.0$.

Hemispherical punch stretching

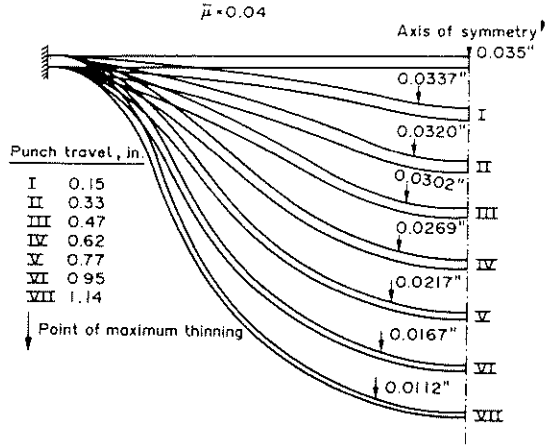

FIG. 13. Relative deformation of the sheet 24 elements $\bar{\mu} = 0.04$.

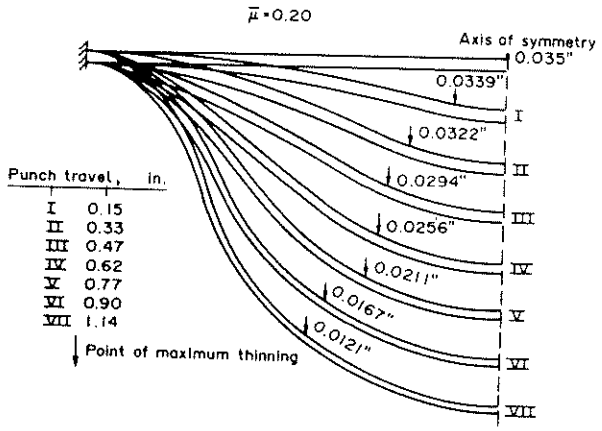

FIG. 14. Relative deformation of the sheet. 24 elements $\bar{\mu} = 0.20$.

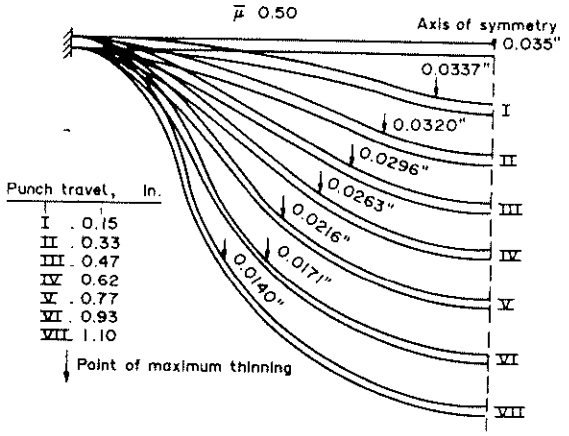

FIG. 15. Relative deformation of the sheet. 24 elements $\bar{\mu} = 0.50$.

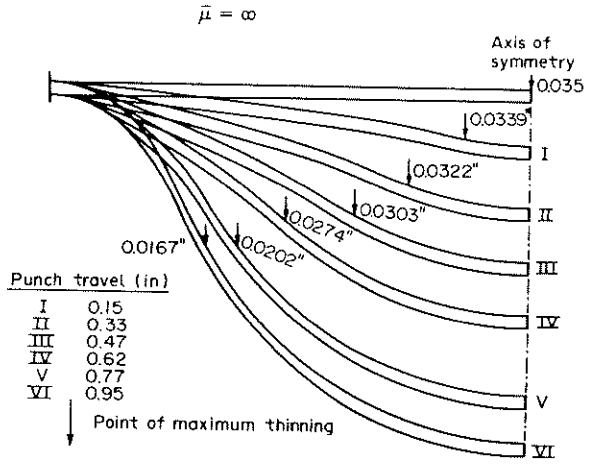

FIG. 16. Relative deformation of the sheet. 24 elements $\bar{\mu} = \infty$.

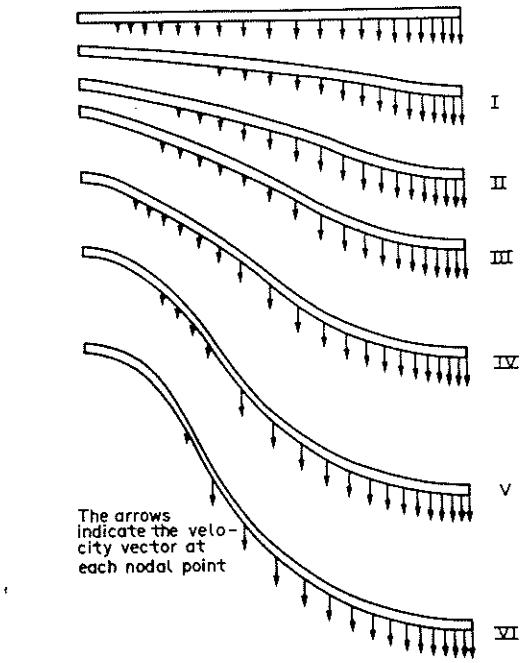

FIG. 17. Different stages of the sheet deformation. 24 elements $\bar{\mu} = \infty$.

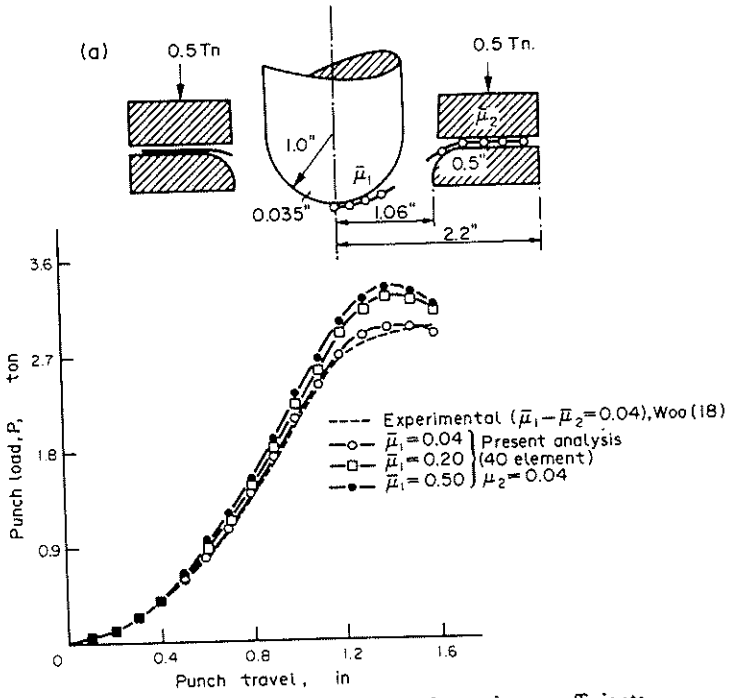

FIG. 18. Punch load/punch travel for various coefficients.

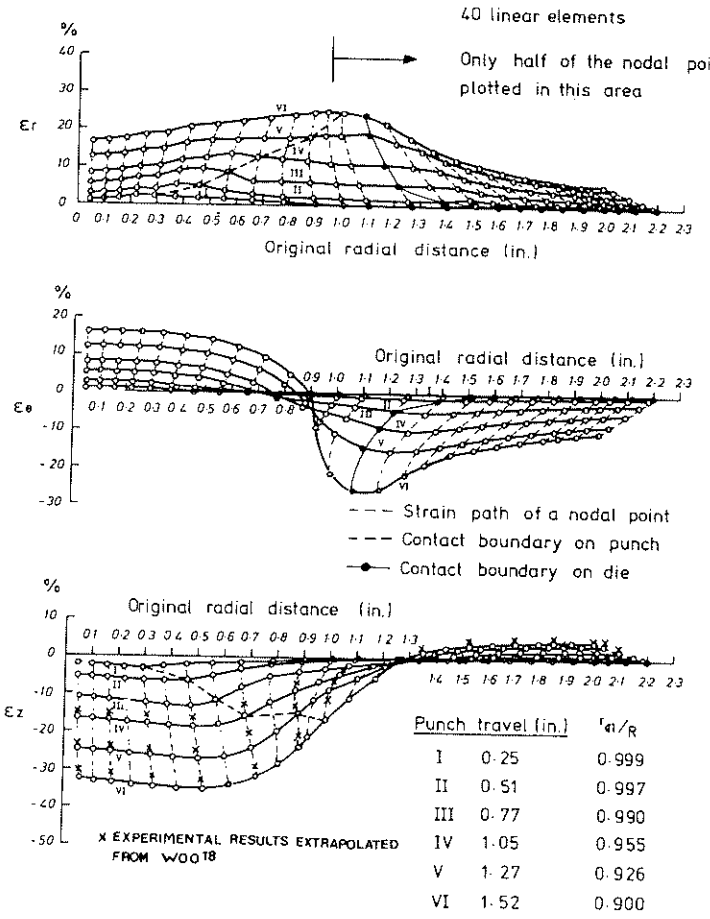

Punch travel (in.)		r_{d1}/R
I	0·25	0·999
II	0·51	0·997
III	0·77	0·990
IV	1·05	0·955
V	1·27	0·926
VI	1·52	0·900

FIG. 19. Strain distributions for $\bar{\mu}_1 = 0.04$, $\bar{\mu}_2 = 0.04$.

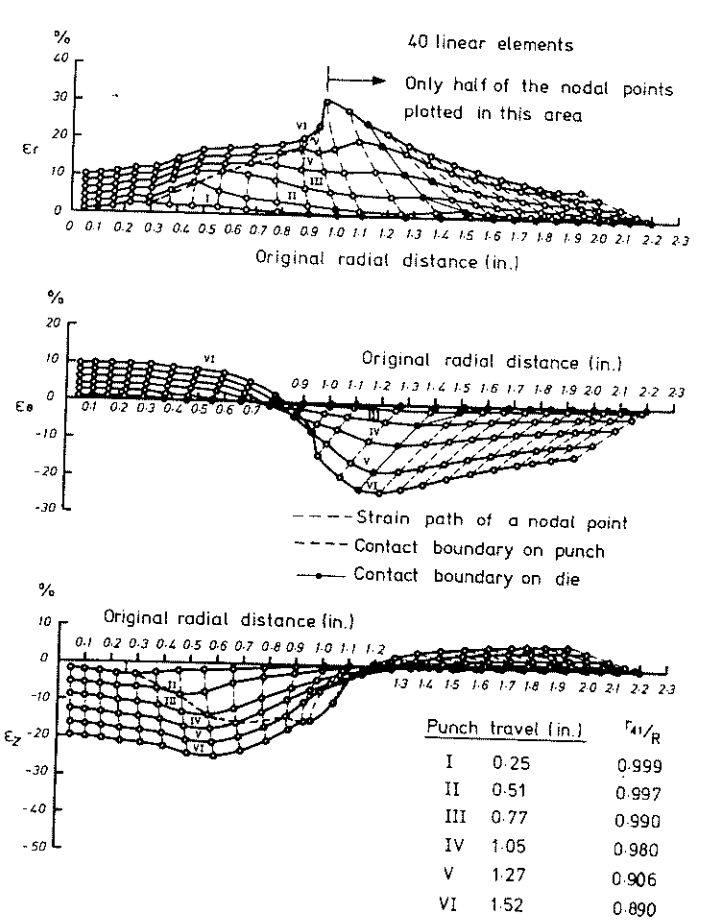

Punch travel (in.)		r_{d1}/R
I	0·25	0·999
II	0·51	0·997
III	0·77	0·990
IV	1·05	0·980
V	1·27	0·906
VI	1·52	0·890

FIG. 20. Strain distributions for $\bar{\mu}_1 = 0.20$, $\bar{\mu}_2 = 0.04$.

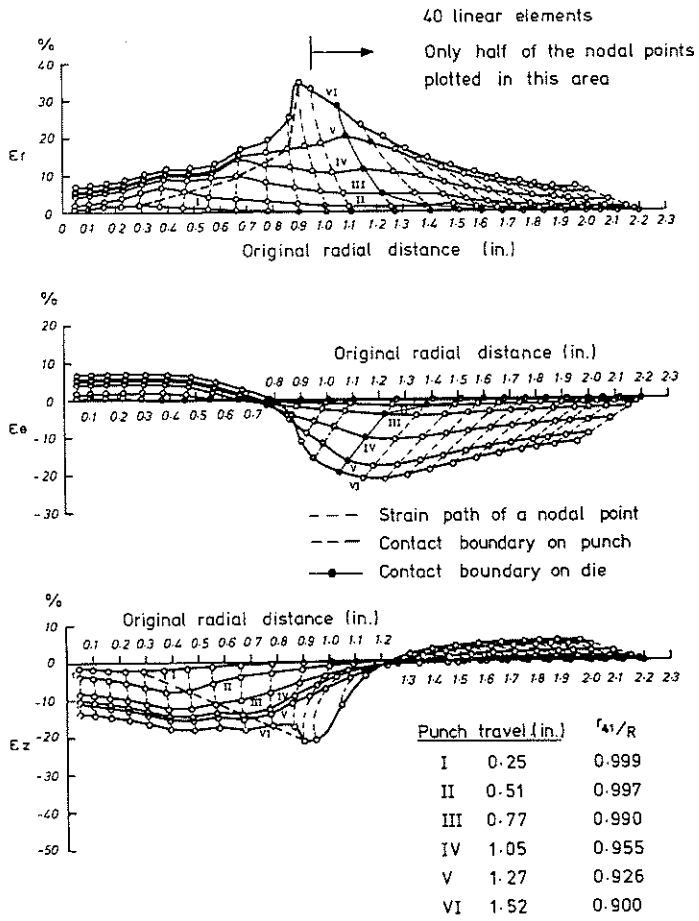

FIG. 21. Strain distributions for $\bar{\mu}_1 = 0.50$, $\bar{\mu}_2 = 0.04$.

coefficients is shown in Figs. 22–24. Also in the same figures the effect of the different friction coefficients over the punch head on the final thickness of the sheet can be noted.

5.3 *Example* 3. *Deep drawing with a flat punch*

Cup drawing from a circular sheet of metal using a flat punch is a common process in the metal forming industry. The problem is very similar to the one previously described and the only difference is the geometry of the punch.

Details of the geometrical configuration of the problem are given in Fig. 26(a) where the stress/effective strain curve of the material is also shown. Experimental results for this problem were provided by the Aluminium Company of America.

Fig. 26(b) shows the punch load versus punch travel and good correlation with the experimental results is obtained.

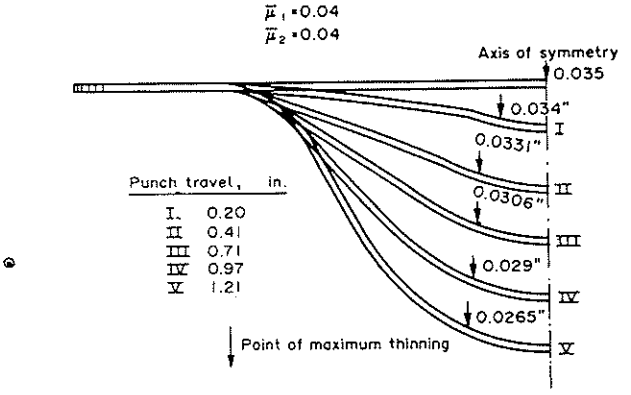

FIG. 22. Relative deformation of the sheet, 40 elements $\bar{\mu}_1 = 0.04$, $\bar{\mu}_2 = 0.04$.

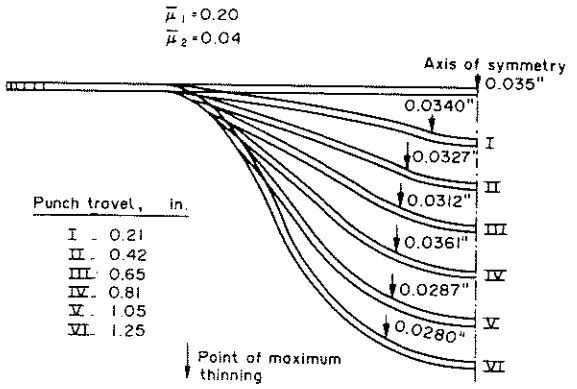

FIG. 23. Relative reformation of the sheet, 40 elements $\bar{\mu}_1 = 0.20$, $\bar{\mu}_2 = 0.04$.

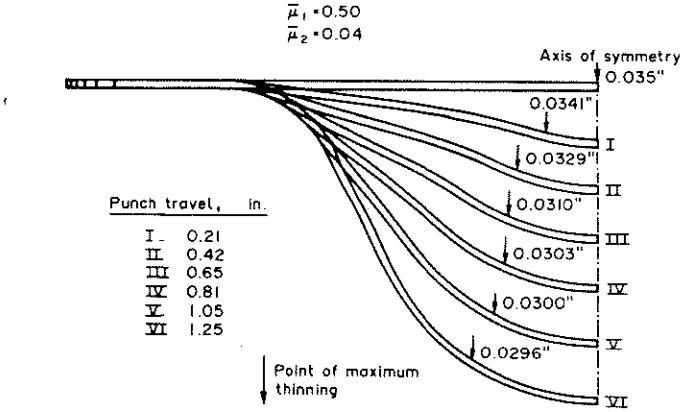

FIG. 24. Relative reformation of the sheet. 40 elements $\bar{\mu}_1 = 0.50$, $\bar{\mu}_2 = 0.04$.

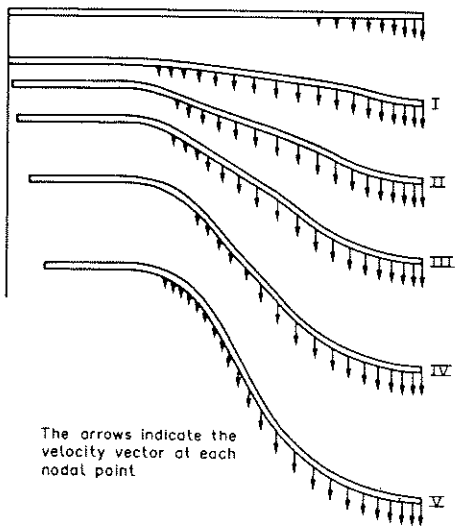

FIG. 25. Different stages of the sheet deformation $\mu_1 = 0.50$, $\bar{\mu}_2 = 0.04$.

Hemispherical deep drawing

The strain distributions for a punch travel of 60 mm are shown in Fig. 26(b). Agreement of numerical results with experimental ones is good.

Finally the deformed geometry at different stages of the process can be seen in Fig. 2(c).

6. GENERAL VISCOUS SHELL FORMULATION

6.1 *Introduction*

Many of the forming processes of thin sheets of metals which occur in the motor car industry are carried out with sheets of arbitrary shape. The problem thus becomes one of large plastic deformation of a non-symmetric thin shell, subjected to the action of a punch which is also of arbitrary shape. The complexity of the problem thus stated is considerable.

Wang and Budianski[29] have suggested a general elasto-plastic finite element procedure based on the non linear theory of membrane shells for calculating the deformations in the stamping of sheet metal by arbitrarily shaped punches and dies. However, in their paper, Wang and Budianksy stress the difficulties of the general process and restrict themselves only to examples of axisymmetric kind similar to the ones presented in the previous chapter using the simplified axisymmetric formulation.

In this section we will show how the viscous shell approach can be formulated to deal with the general deformation of sheets of metal. Only isotropic material will be treated here for simplicity but more complex anisotropic situations can be treated in a similar manner taking into account the rotations of the principal axes of anisotropy.

The general viscous shell formulation will be obtained, as for the axisymmetric case of last sections, by analogy with the incompressible elastic shell theory. The elastic shell formulation chosen here is identical to that used by Ahmad[49, 53] and it will be briefly described in next section.

6.2 *Basic shell formulation*

The shell theory used is based on the following assumptions:

(1) deflections are small

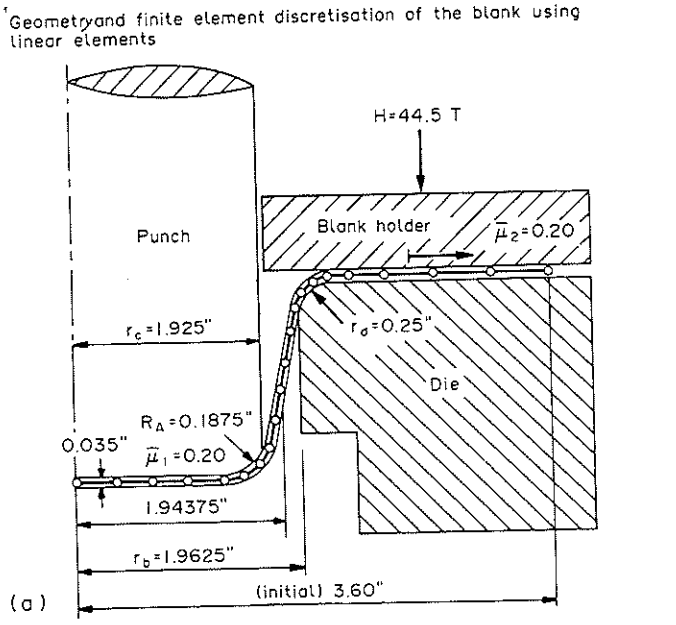

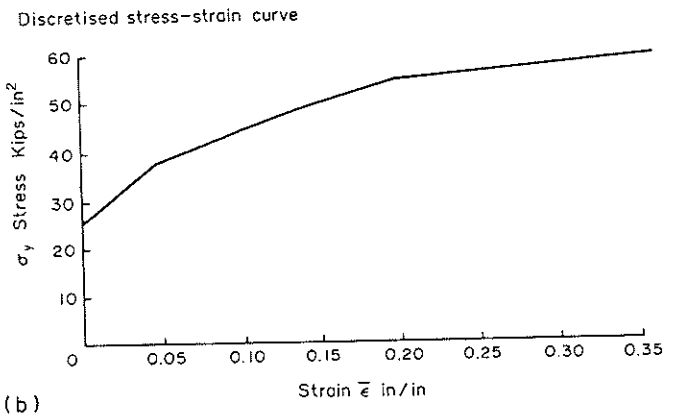

Fig. 26(a).

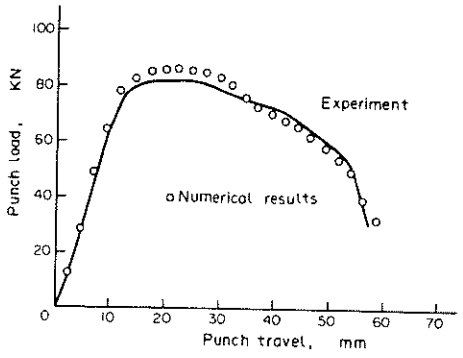

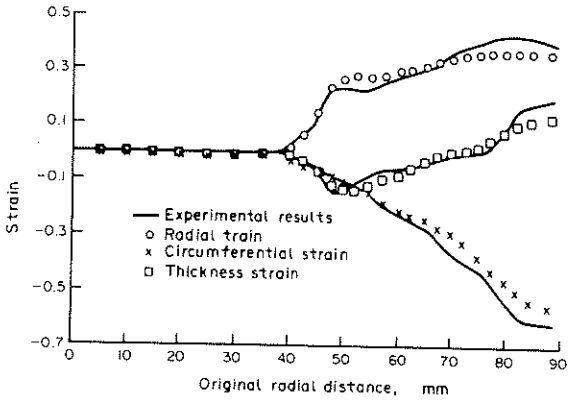

(b)

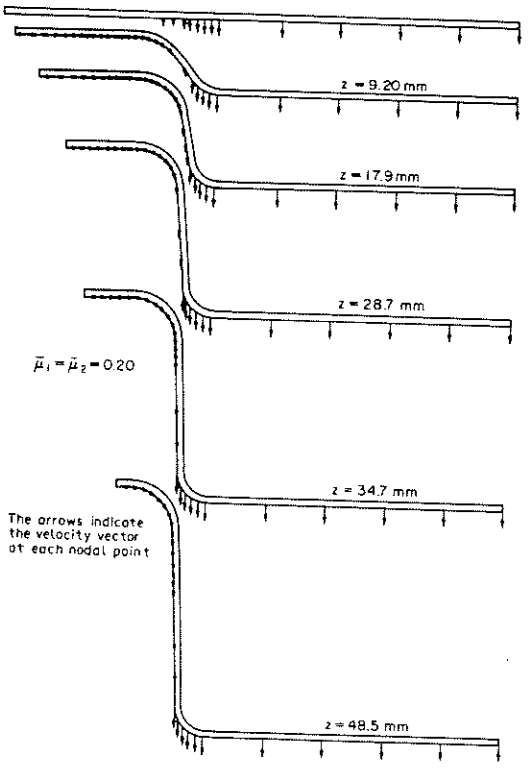

(c)

FIG. 26. (a) Flat nosed punch. Geometry and discretised stress–strain curve. Alloy No. 84. (b) Flat nosed punch. Strain distributions for punch travel = 60 mm. (c) Flat bottom punch. Deformation of different stages.

(2) normals the midsurface before deformation remain straight but not necessarily normal to the midsurface after deformation

(3) the normal stress is negligible

A local coordinate system (x', y', z') is adopted in which the z' direction coincides with the normal to the shell midsurface and

$$\mathbf{u}' = \begin{Bmatrix} u' \\ v' \\ w' \end{Bmatrix} \tag{59}$$

are the displacements in the x', y' and z' directions, as shown in Fig. 27. Since the stress normal to the midsurface, $\sigma'_{z'}$ is assumed to be zero, it is possible to eliminate the normal strain $\epsilon_{z'}$ from the stress/strain relationships. Thus, for an isotropic material [49, 53].

$$\boldsymbol{\sigma}_1 = \mathbf{D}_1 \boldsymbol{\epsilon}_1; \quad \boldsymbol{\sigma}_2 = \mathbf{D}_2 \boldsymbol{\epsilon}_2 \tag{60}$$

in which

$$\boldsymbol{\sigma}_1 = [\sigma'_{x'}, \sigma_{y'}, \tau_{x'y'}]^T; \quad \boldsymbol{\epsilon}_1 = \left[\frac{\partial u'}{\partial x'}, \frac{\partial v'}{\partial y'}, \frac{\partial u'}{\partial y'} + \frac{\partial v'}{\partial x'}\right]^T \tag{61}$$

$$\boldsymbol{\sigma}_2 = [\tau_{x'z'}, \tau_{y'z'}]^T; \boldsymbol{\epsilon}_2 = \left[\frac{\partial w'}{\partial z'} + \frac{\partial w'}{\partial z'}, \frac{\partial w'}{\partial z'} + \frac{\partial w'}{\partial y'}\right]^T \tag{62}$$

$$\mathbf{D}_1 = \frac{2G}{1-\nu}\begin{bmatrix} 1 & \nu & 0 \\ \nu & 1 & 0 \\ 0 & 0 & \dfrac{1-\nu}{2} \end{bmatrix}; \mathbf{D}_2 = \frac{G}{K}\begin{bmatrix} 1 & 0 \\ 0 & 1 \end{bmatrix} \tag{63}$$

where G is the shear modulus, is the Poisson's ratio and K is a shear correction factor due to non-uniform shear distribution (we have taken $K = 5/6$).

The virtual work statement can be written as

$$\int_\Omega \delta\boldsymbol{\epsilon}_1{}' \mathbf{D}_1 \boldsymbol{\epsilon}_1 \, d\Omega + \int_\Omega \delta\boldsymbol{\epsilon}_2{}' \mathbf{D}_2 \boldsymbol{\epsilon}_2 \, d\Omega = \int_\Omega \delta\mathbf{u}'^T \bar{\mathbf{b}}' \, d\Omega + \int_\Gamma \delta\mathbf{u}'^T \bar{\mathbf{t}} \, d\Gamma \tag{64}$$

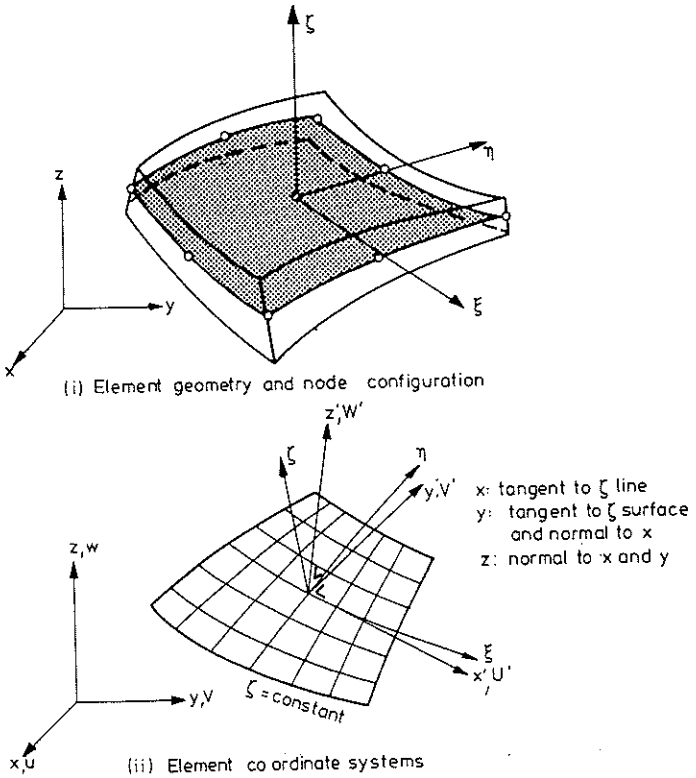

FIG. 27. The 'thick' shell element.

in which the body forces are given as

$$\mathbf{b}' = [bx', by', bz']^T$$

and the boundary traction as

$$\bar{\mathbf{t}}' = [\bar{t}x', \bar{t}y', \bar{t}z']^T \tag{66}$$

6.3 *"Thick" shell elements*

From the assumption (2) of the shell theory used, it follows that the displacements in the global (cartesian) coordinate direction, x, y and z can be represented by the relationship

$$\mathbf{u} = \sum \mathbf{N}_i(\xi, \eta, \zeta)\mathbf{a}_i \tag{67}$$

in which the vector of nodal displacement parameters is:

$$\mathbf{a}_i = [u_i, v_i, w_i, \bar{\alpha}_i, \bar{\beta}_i]^T \tag{68}$$

where u_i, v_i and w_i are the nodal displacements in the global directions and $\bar{\alpha}_i$ and β_i are nodal normal rotations about y' and x' directions respectively (see Fig. 27). The shape function matrix can be written as

$$N_i(\xi, \eta, \zeta) = [N_i(\xi, \eta)\mathbf{I}_3, \zeta \frac{h_i}{2} \mathbf{V}_{\alpha i} N_i(\xi, \eta), \zeta \frac{h_i}{2} \mathbf{V}_{\beta i} N_i(\xi, \eta] \tag{69}$$

in which $\mathbf{I}_3$ is e 3×3 identity matrix, h_i is the shell thickness at the node i, $\mathbf{V}_{\alpha i}$ and $\mathbf{V}_{\beta i}$ are unit vectors in two orthogonal directions in the tangent plane to the shell midsurface at node i and $N_i(\xi, \eta)$ is the shape function associated with node i.

To obtain the strains of equations (64) and (65) in terms of the nodal displacements, $\mathbf{a}_i$, and the local coordinates ξ, η, ζ two sets of transformations are necessary.

First, the derivatives of displacements u, v, and w are obtained with respect to ξ, η, ζ, and then changed to those with respect to x, y and z by using the standard expressions

$$\frac{\partial \mathbf{u}}{\partial \mathbf{x}} = \mathbf{J}^{-1} \frac{\partial \mathbf{u}}{\partial \boldsymbol{\zeta}}; \quad \boldsymbol{\xi} = [\xi, \eta, \zeta]^T; \tag{70}$$

where $\mathbf{J}$ is the Jacobian matrix. Second, since the strains of interest in the present case are in the local system of coordinates, we have to transform the global derivatives of displacements into the local. This can be done by the following operation:

$$\frac{\partial \mathbf{u}'}{\partial \mathbf{x}'} = \boldsymbol{\theta}^T \frac{\partial \mathbf{u}}{\partial \mathbf{x}} \boldsymbol{\theta} \tag{71}$$

where $\boldsymbol{\theta}$ is an orthogonal matrix formed by the directions of the local axes. Details of this transformation can be found in Refs. [49] and [60].

Strain-displacement relationships can be written as

$$\boldsymbol{\epsilon}_1 = \sum \mathbf{B}_{1i}\mathbf{a}_i \quad \text{and} \quad \boldsymbol{\epsilon}_2 = \sum B_{2i}\mathbf{a}_i \tag{72}$$

Substituting equations (72) into the virtual work statement equation (64) the stiffness equations can be obtained. Typical terms in the stiffness matrix and associated load vectors are given as:

$$\mathbf{K}_{ij} = \int_\Omega \mathbf{B}_{1i}^T \mathbf{D}_1 b_{1j} \, d\alpha + \int_\Omega \mathbf{B}_{2i}^T \mathbf{D}_2 \mathbf{B}_{2j} \, d\Omega = \mathbf{K}_{1ij} + \mathbf{K}_{2ij} \tag{73}$$

$$\mathbf{f}_i = \int_\Omega \mathbf{N}_i^T \mathbf{b} \, d\Omega + \int_\Gamma \mathbf{N}_i^T \bar{\mathbf{t}} \, d\Gamma. \tag{74}$$

All the points about the influence of the shear terms of the stiffness matrix K_{ij} (i.e. the terms contained in matrix K_{2ij} of equation (73)) when the shell thickness becomes small, mentioned earlier for the axisymmetric formulation are again applicable. There are several techniques for improving the performance of the different 'thick' shell elements for thick and thin shell analysis. We will not here go into details of this interesting problem but simply mention that if a nine noded Lagrangian element, such as that of Fig. 27, is used, a selective integration scheme for the numerical integration of matrix $\mathbf{K}_{ij}$ which involves a $3 \times 3 \times 2$ Gaus–Legendre rule for $\mathbf{K}_{1ij}$ and a $2 \times 2 \times 2$ rule for $\mathbf{K}_{2ij}$ should be used for the success of the formulation for both thick and very thin shell situations. More information about this problem can be found in Refs. [50]–[63].

It is also worth mentioning here that the above formulation is only valid for flat or smoothly curved structures (i.e. without kinks or branching). However, when dealing with kinked shell situations, or multiple junctions, it is necessary to take into account the rotation about an axis normal to the midsurface and to consider an assembly in six degrees of freedom. This is done by introducing the zero in-plane rotational stiffness locally and then transforming to the global frame. To overcome the difficulty of the singularity of

the stiffness matrix which arises when the element boundaries are joined in a co-planar manner, an artificial in-plane rotational stiffness in the element stiffness formulation can be introduced.

In this paper a procedure similar to that suggested in Ref. [50] is used. Two different types of nodes are defined, i.e. co-planar and non-co-planar nodes. A co-planar node is defined as one where all the elements share the same tangent plane. A non-co-planar node is one at which they do not have a common tangent plane. At the co-planar nodes the nodal rotations are α_i, β_i, θ_i in the local frame, where θ_i is the in-plane rotation. Now an artificial rotational stiffness is introduced in the coefficient of the stiffness matrix corresponding to θ_i to avoid singularity. At the non-co-planar nodes the nodal variables are the nodal displacements and rotations transformed into the global coordinate system. With this procedure the computational effort of transforming the local rotations of the coplanar nodes to the global system can be avoided. More details of this can be found in Ref. [50].

6.4 *General viscous shell formulation*

The viscous shell formulation will be obtained by analogy with the elastic shell formulation previously described, assuming incompressible behaviour of the material ($\nu \to 0.5$). The general procedure is identical to that followed throughout this paper for the viscous flow/elasticity analogy. The vector of local and global displacements $\mathbf{u}'$ and $\mathbf{u}$ (equations (59 and 67) become now the vectors of local and global velocities, and the local strain vectors $\boldsymbol{\epsilon}_1$ and $\boldsymbol{\epsilon}_2$ (equations 61 and 62) become the strain rate vectors $\dot{\boldsymbol{\epsilon}}_1$ and $\dot{\boldsymbol{\epsilon}}_2$.

The stress/strain rate relationships for *isotropic* materials can be obtained simply by putting $\nu = 0.5$ in equations (63) and substituting for the shear modulus, G, the viscosity, μ. This results in the following relations:

$$\boldsymbol{\sigma}_1 = \mathbf{D}_1 \dot{\boldsymbol{\epsilon}}_1 \quad \text{and} \quad \sigma_2 = \mathbf{D}_2 \dot{\boldsymbol{\epsilon}}_2, \tag{75}$$

where definitions and strains are similar to equations (61) and (62).

and

$$\mathbf{D}_1 = 2\mu \begin{bmatrix} 2 & 1 & 0 \\ 1 & 2 & 2 \\ 0 & 0 & 1 \end{bmatrix}; \quad D_2 = \mu \begin{bmatrix} 1 & 0 \\ 0 & 1 \end{bmatrix}. \tag{76}$$

For pure plastic flow only, the viscosity is given by the standard expression, equation (9), as

$$\mu = \frac{\sigma_y}{3\sqrt{4\dot{\epsilon}_x^2 + 4\dot{\epsilon}_y^2 + 4\dot{\epsilon}_x\dot{\epsilon}_j + \gamma_{xy}^2 + \gamma_{yz}^2 + \gamma_{xy}^2)}}. \tag{77}$$

The virtual work equation equivalent to equation (64) can once again be written providing the basis for the finite element discretization.

6.5 *Element discretization*

This follows exactly the lines explained for the elastic case. The velocity vector in the global system $\mathbf{a}$, is expressed in terms of trial functions $\mathbf{N}_i$ and nodal velocity vectors $\mathbf{a}$ by

$$\mathbf{u} = \sum \mathbf{N}_i \mathbf{a}_i \tag{78}$$

where $\mathbf{u}$, N_i and $\mathbf{a}_i$ are defined in equations (67)–(69).

Strain rate nodal velocity relationships can then be similarly obtained from equation (72), as

$$\dot{\boldsymbol{\epsilon}}_1 = \sum \mathbf{B}_{1i}\mathbf{a}_i; \quad \dot{\boldsymbol{\epsilon}}_2 = \sum \mathbf{B}_{2i}\mathbf{a}_i. \tag{79}$$

Following standard procedures [52], a system of equations is obtained of typical form.

$$\mathbf{K}\mathbf{a} = \mathbf{f} \tag{80}$$

where $\mathbf{K}$ and $\mathbf{f}$ are given by equations (73) and (74) respectively.

All the points mentioned in the elastic shell section about matrix $\mathbf{K}$ are repeatable here.

Once again, dependence of μ on the velocity field makes the problem non-linear and the solution of system of equations (80) follows using a direct iteration scheme (see equation 11).

6.6 *Geometry updating*

Due to the difficulty of dealing with three dimensional shapes we have chosen a simple criterion to determine the step size Δt. To calculate the time increment for which the first node in the non-contacting region comes into contact with the punch, a procedure similar to that described previously for the axisymmetric case has been followed. The coordinates and the velocities of point j (see Fig. 28) in the cartesian system at a time t are (xj, yj, zj) and (uj, vj, wj) respectively. We shall only consider a simple case of a hemispherical punch. The surface equation for this is

$$x^2 + y^2 + (R_p - z)^2 = R_p^2. \tag{81}$$

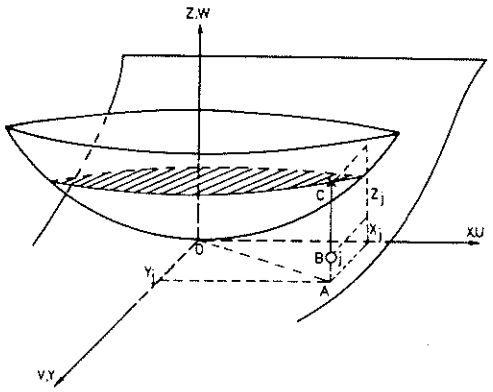

FIG. 28. General thin sheet forming problem.

From Fig. 28 we see that node B will come into contact with the punch if at a time $t+\Delta t$, $AB = BC$, i.e.

$$z_j + (w_f - \omega_j)\Delta t = R_p - \sqrt{(R_p^2 - AO^2)} \tag{82}$$

where ω_p is the vertical velocity of the punch and

$$AO = \sqrt{[(z_j + u_j\Delta t)^2 + (y_j + v_j\Delta t)]^2}. \tag{83}$$

Equation (86) must be solved for the value of Δt. We adopt here a direct iteration Euler scheme. This gives, for the nth iteration

$$\Delta t^n = \frac{1}{(w_p - w_j)}[R_p - z_j - \sqrt{(R_p^2 - (AO^{n-1})^2)} \tag{84}$$

where

$$AO^{n-1} = \sqrt{[(x_j + u_j\Delta t^{n-1})^2 + (y_j + v_j\Delta t^{n-1})^2]}. \tag{85}$$

6.7 *Treatment of friction*

Friction effects between sheet and punch interface can be taken into account in a way similar to that explained for the axisymmetric case. The friction coordinate system is now defined for each node as the average of the local coordinate system direction corresponding to the different elements meeting at that particular node. For smooth shells the friction coordinate system should coincide with the local coordinate system (x', y', z' in Fig. 27) for each node.

The nodal displacements in the global system u_i, v_i, and w_i are related to the displacements in the friction system $\bar{u}_i$, $\bar{v}_i$, and $\bar{w}_i$ as

$$\mathbf{u}_i = \mathbf{T}_i\bar{\mathbf{u}}_i$$

where T_c is the 3×3 cosine matrix of the friction system. The stiffness matrix in the friction system $\bar{T}_i$ is given by the standard relation

with

$$\bar{T}_i = \begin{bmatrix} T_i & 0 \\ 0 & \mathbf{I} \end{bmatrix} \tag{87}$$

where I is a 2×2 unity matrix for smooth shells, or a 3×3 unity matrix, if a kinked or branched shell solution is attempted. (Note that only the nodal displacements have been transformed).

The stiffness equation in the friction system now has the form

$$\bar{\mathbf{K}}\bar{\mathbf{a}} = \bar{\mathbf{f}} \tag{88}$$

where

$$\bar{\mathbf{a}}_i = [\bar{u}_i, \bar{v}_i, \bar{w}_i, \alpha_i, \beta_i]^T \tag{89}$$

and

$$\bar{f}_i = [\bar{U}_i, \bar{V}_i, \bar{W}_i, M_{\alpha i}, M_{\beta i}]^T \tag{90}$$

here V_i, $\bar{V}_i$ and $\bar{W}_i$ are the reactions in the directions of the nodal displacements $\bar{u}_i$, $\bar{v}_i$ and $\bar{w}_i$ respectively.

Once the forces in the assumed slipping directions have been found the friction conditions can be checked using the algorithm described earlier.

It is noted that the procedure described above has been implemented in the computer program developed for the general analysis of deformations of thin sheets of metal, and it has been successfully tested. However, no slippage between tool and sheet has been assumed in the examples analysed in this paper as computational costs are high and convergence slow when this is taken into account. Further developments are in progress.

6.8 *Examples*

The effectiveness of the formulation, described in the previous section has been tested with two simple examples of hemispherical stretch forming. An axisymmetric solution is attempted first and results are compared with those obtained in the previous chapter using the axisymmetric formulation. The second problem is the hemispherical punch stretching of a square blank clamped at its edges and shows how non-symmetric solutions can be attempted successfully with the general viscous shell formulation.

6.9 *Example* 1. *Hemispherical punch stretching of a circular blank*

The first problem chosen is identical to the first problem of the axisymmetric section. The die radius has been taken equal to zero for simplicity. The punch and blank geometry can be seen in Fig. 29. The stress/effective strain curve of the material is identical to that shown in Fig. 6. Due to the symmetry of the problem, only one quarter of a circle has been analysed. Fig. 29 shows the finite element mesh used and the boundary conditions. Rigid contact between punch and sheet has been assumed.

Results for the punch load/punch travel curve and for the thickness strain distributions at different stages of the deformation can be seen in Fig. 29. Good agreement with results obtained with the axisymmetric formulation previously described is obtained.

6.10 *Example* 2. *Hemispherical punch stretching of a square blank*

This final example shows the ability of the viscous shell formulation to deal with general non-axisymmetric sheet metal forming situations. The problem analysed is essentially similar to the one studied in the previous example but now with a square blank instead of a circular one. Details of the geometry of the problem and finite element discretisation can be seen in Fig. 30. The stress-effective strain curve of the material is, similarly as for the previous example, identical to that shown in Fig. 6.

Numerical results for the punch load/punch travel curve and the thickness strain distributions at the symmetry line for different stages of the deformation can be seen in Fig. 30. No experimental or alternative numerical results are available for this type of problem so no comparison of results is shown.

7. CONCLUSIONS

The "viscous shell formulation", based on its analogous elastic shell formulation, is a versatile and successful method for the analysis of thin sheet metal deformation problems.

For axisymmetric situations the linear element has proved to be cheap and accurate for the analysis of cup forming processes. The comparison of numerical results with experimental data has been good. In particular the algorithm to simulate friction reproduces very realistic friction effects on the maximum load and the strain distributions.

The general viscous shell formulation allows the study of the deformation of thin sheets of metal with arbitrary shape. The simple examples solved show the applicability of the method to deal with such complex problems and it opens a wide field of possibilities for research.

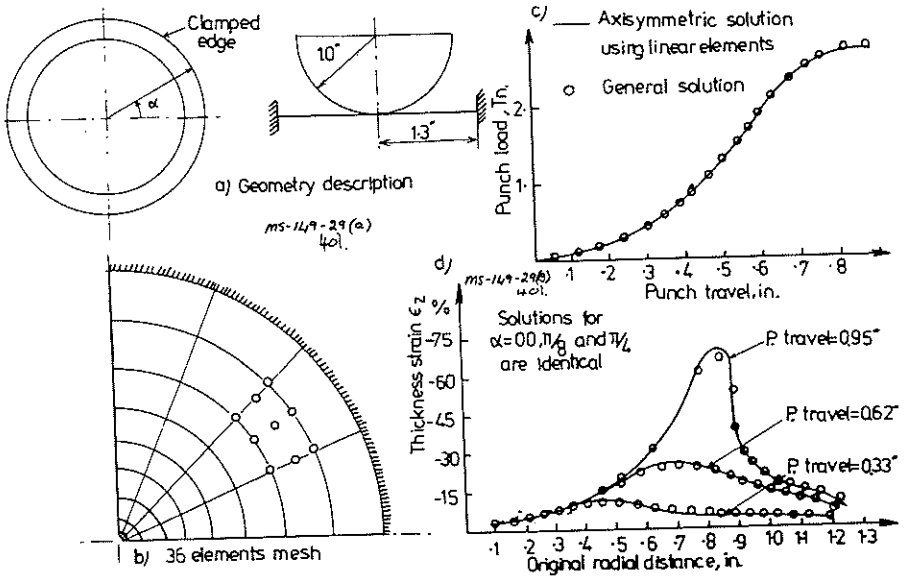

FIG. 29. Hemispherical punch stretching of a circular sheet of metal. Rigid contact.

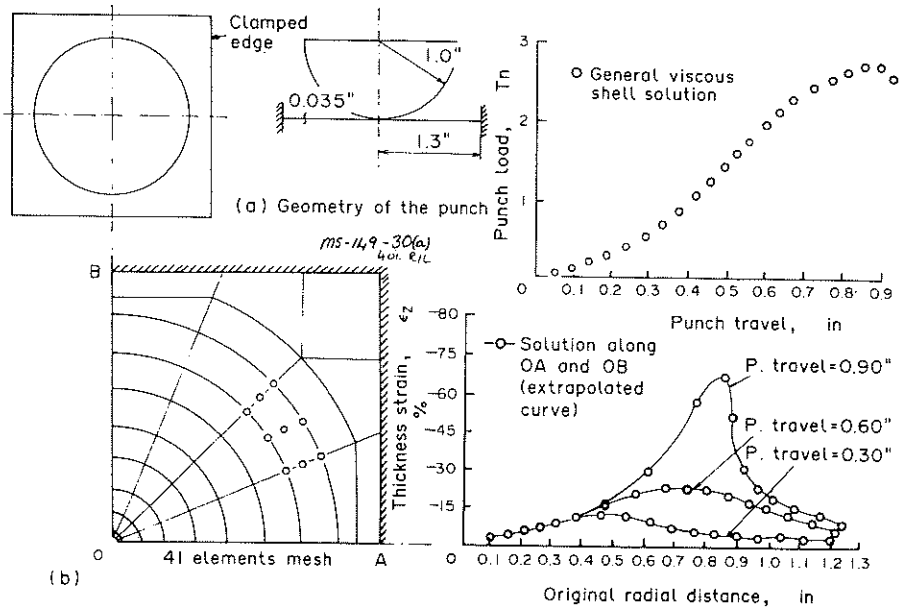

FIG. 30. Hemispherical punch stretching of a square sheet of metal. Rigid contact.

Acknowledgment—The authors would like to thank ALCOA FOUNDATION of U.S.A. for the financial support of E. Oñate during this work.

REFERENCES

1. S. P. KEELER, Understanding sheet metal formability. *Machinery* **74**, (1968).
2. S. P. KEELER, Circular grid system—a valuable aid for evaluating sheet metal formability. SAE Paper No. 680092, 1968.
3. S. P. KEELER and W. A. BACKOFEN, Plastic instability and fracture in sheets stretched over rigid punches. *Trans. ASM*, **56**, 25 (1963).
4. G. M. GOODWIN, Applications of strain analysis to sheet metal forming problems in the press shop. SAE Paper No. 680093, 1968.
5. S. S. HECKER, Formability of high-strength low-allow steel sheets. *Met. Engng Quart.* **13**, 42 (1973).
6. S. P. KEELER, Forming limit criteria—sheets. *Pres. 21st Sagamore Army Materials Res. Conf.*, Lake Roquette, N.Y., 13–16 August, 1974.
7. Y. TOZAWA, M. NAKAMURA and I. SHINKAI, Yield loci for prestrained steel sheets. *Proc. ICSTIS*, Section 5, Supplement to *Trans. ISIJ*, **11**, 936 (1971).
8. K. KANEKO, K. IKEGAMI and E. SHIRATORI, The yield condition and flow rule of a metal for the various pre-strain paths. *Bull. JSME* **19**, 577 (1975).
9. E. SHIRATORI, K. IKEGAMI and F. YOSHIDA, The subsequent yield surfaces after proportional preloading of the Tresca-type material. *Bull. JSME* **16**, 1122 (1976).
10. Y. OHASHI, K. KAWASHIMA and N. MORI, On proportional combined loading tests of an aluminium alloy and its analytical formulation. *J. Engng Mater. Techn.* **98**, 282, (1976).
11. J. A. NEWNHAM, Sheet metal working lubrication. *Metal Deformation Processes, Friction and Lubrication* (Edited by J. A. Schey). Marcel Dekker, New York (1970).
12. B. KAFTANOGLU, Determination of coefficient of friction under conditions of deep drawing and stretch forming. *Wear* **25**, 177 (1973).
13. W. T. LANKFORD, S. C. SNYDER and J. A. BAUSCHER, New criterua for predicting the press performance of deep drawing sheets. *Trans. ASM* **42**, 1197 (1950).
14. R. L. WHITELY, The importance of directionality in drawing quality steel. *Trans. ASM* **52**, 154, 1960.
15. D. B. KOISTIEN N. M. WANG (Eds), Mechanics of sheet metal forming. *Material Behaviour and Deformation Analysis*. Plenum Press, New York (1978).
16. S. Y. CHUNG and J. W. SWIFT, Cup forming from a flat blank—1. Experimental investigations—2, Analytical investigations. *Proc. Inst. Mech. Engrs* **165**, 199 (1951).
17. D. M. WOO, Analysis of the cup drawing process. *J. Mech. Engng Sci.* **6**, 116 (1964).
18. D. M. WOO, On the complete solution of the deep drawing problem. *Int. J. Mech. Sci.* **10**, 83 (1968).
19. D. M. WOO, The stretch forming test. *The Engineer* **220**, 876 (1965).
20. R. HILL, *The Mathematical Theory of Plasticity*. Oxford University Press (1950).
21. N. M. WANG, Large plastic deformation of a circular sheet caused by punch stretching. *J. Appl. Mech.* **37**, 431 (1970).
22. B. KAFTANOGLU and J. M. ALEXANDER, Outer quasi-static axisymmetric stretch forming. *Int. J. Mech. Sci.* **12**, 1065 (1970).
23. G. G. MOORE and J. F. WALLACE, The effect of anisotropy on instability in sheet metal forming. *J. Inst. Metals*, **93**, 33 (1964).

24. D. C. CHIANG and S. KOBAYASHI, The effect of anisotropy and work hardening characteristics on the stress and strain distribution in deep drawing. *J. Engng. Ind.* **88**, 443 (1966).
25. A. S. WIFI, An Incremental complete solution of the stretch forming and deep drawing of a circular blank using a hemispherical punch. *Int. J. Mech. Sci.* (1975).
26. Y. YAMADA, *Recent Advances in Matrix Method of Structural Analysis and Design.* (Edited by R. Gallagher, Y. Yamada and J. T. Oden) University of Alabama Press, Birmingham (1971).
27. Y. YAMADA, Studies on formability of sheet metals. *Inst. Ind. Sci., Tokyo*, **11**, 242 (1961). In Japanese with English summary.
28. H. GOTOH, A finite element analysis of general deformation of sheet metal. *Int. J. Num. Meth. Engng* **8**, 731 (1974).
29. N. M. WANG and B. BUDIANSKI, Analysis of sheet metal stamping by a finite element method. *J. Appl. Mech. Trans ASME* **45**, 73 (1976).
30. S. FUKUI, H. YURI and K. YOSIDA, Analysis for deep drawing of cylindrical shell based on total strain theory and some formability tests. *Aeronauti, Res., Inst. Tokyo* **24**, 332, (1958).
31. S. P. KEELER, Sheet metal stamping technology. *Need for Fundamental Understanding. Mechanics of Metal Forming* (Edited by D. P. Koistinen and N. M. Wang), pp. 3–18. Plenum Press, New York (1978).
32. O. C. ZIENKIEWICZ, P. C. JAIN and E. ONATE, Flow of solids during forming and extrusion. Some aspects of numerical solutions. *Int. J. Solids Structures* **14**, 15–38 (1978).
33. G. Y. GOON, P. I. POLUCHIN, W. P. POLUCHIN and B. A. PRUDCOWSKY, *The Plastic Deformation of Metals.* Metallurgica, Moscow (Russian), (1968).
34. O. C. ZIENKIEWICZ and P. N. GODBOLE, Flow of plastic and visco-plastic solids with special reference to extrusion and forming processes. *Int. J. Num. Meth. Engng* **8**, 3–16 (1974).
35. O. C. ZIENKIEWICZ and P. N. GODBOLE, Viscous incompressible flow. *Int. Conf. on Finite Element Methods in Flow Problems*, Swansea 1974 (Edited R. H. Gallagher, J. T. Oden, C. Taylor and O. C. Zienkiewicz) Wiley, New York (1975).
36. O. C. ZIENKIEWICZ and P. N. GODBOLE, A penalty function approach to problems of plastic flow of metals with large surface deformation. *J. Strain Anal.* **10**, 180–185, I. Mech. E. (1975).
37. G. C. CORNFIELD and R. H. JOHNSON, Theoretical predictions of plastic flow in hot rolling including the effect of various temperature distributions. *J. Iron and Steel Inst.* **211**, 567–573 (1973).
38. C. H. LEE and S. KOBAYASHI, New solutions to rigid-plastic deformation problems using a matrix method. *Int. Eng. Ind. Trans. ASME* **95**, 865 (1973).
39. O. C. ZIENKIEWICZ, Viscoplasticity, plasticity, creep and viscoplastic flow (problems of small, large and continuing deformation). *Int. Conf. in Non-Linear Mech.*, Texas, 1974.
40. R. S. DUNHAM, On application of the finite element method to limit analysis. Computational methods in non-linear mechanics. *Int. Conf. on Computational Methods in Non-Linear Mech.*, Texas, 1974.
41. J. N. H. PRICE and J. M. ALEXANDER, The finite element analysis of two high temperature metal deformation processes. *2nd Int. Symp. Finite Element in Flow Problems*, Santa Margherita Ligure (Italy), pp. 715–728, June 1976.
42. P. C. JAIN, Plastic flow in solids (static quasistatic and dynamic situations including temperature effects). Ph.D Thesis, University College of Swansea, Oct. 1976.
43. E. ONATE and O. C. ZIENKIEWICZ, Plastic flow of axisymmetric thin shells as a non Newtonian flow problem and its application to stretch forming and deep drawing problems. *Proc. IDDRG, 10th Biennial Congress*, University of Warwick, England, 1978.
44. O. C. ZIENKIEWICZ and E. ONATE, Finite element solutions of some problems of metal forming using the plastic flow approach. *Proc. Int. Congress on Numerical Meth. Engng.* Organised by the Group for Development of Numerical Methods for Engineering GAMNI, Paris, 27th November 1978.
45. O. C. ZIENKIEWICZ, E. ONATE and J. C. HEINRICH, Plastic flowin metal forming. *Proc. Winter Ann. Meeting ASME*, San Francisco, California, Dec. 1978.
46. E. ONATE, Plastic flow in metals. I. Thermal coupling behaviour. II. Thin sheet forming. Ph.D. Thesis. University College of Swansea. C/Ph/51/78, 1978.
47. (a) P. PERZYNA, Fundamental problems in visco plasticity. *Recent Advances in Applied Mechanics*, Chap. 9, pp. 243–377. Academic Press, New York (1966). (b) O. C. ZIENKIEWICZ and I. C. CORMEAU, Visco-plasticity, plasticity and creep in elastic solids: A unified numerical solution approach. *Int. J. Num. Meth. Engng* **8**, 821–845 (1974).
48. O. C. ZIENKIEWICZ, J. BAUER, K. MORGAN and E. ONATE, A simple and efficient element for axisymmetric shells. *Int. J. Num. Meth. Engng* **11**, 1545–1559 (1977).
49. S. AHMAD, B. M. IRONS and O. C. ZIENKIEWICZ, Analysis of thick and thin shells and plate structures. *Int. J. Num. Meth. Engng* **2**, 419–451 (1970).
50. O. C. ZIENKIEWICZ, J. TOO and R. L. TAYLOR, Reduced integration techniques in general analysis of plates and shells. *Int. J. Num. Meth. Engng* **3**, 279–290 (1971).
51. O. C. ZIENKIEWICZ and E. HINTON, Reduced integration, function smoothing and non-conformity in finite element analysis. *J. Franklyn Inst.* **302**, 443–461 (1976).
52. O. C. ZIENKIEWICZ, *The Finite Element Method.* 3rd Edn, McGraw-Hill, New York (1977).
53. S. AHMAD, Curved finite elements in the analysis of solid shell and plate structures. Ph.D. Thesis, University College of Swansea. C/Ph/7/69. 1969.
54. A. K. GHOSH, Plastic flow properties in relation to localized neching in sheets. *Mechanics of Metal Forming* (Edited by D. P. Koistinin and N. M. Wang), Plenum Press, New York (1978).
55. A. K. GHOSH, Ph.D. Thesis, Dept. of Metallurgy and Materials Science, MIT, Cambridge, Mass, 1972.
56. J. H. KIM, S. I. OH and S. KOBAYASHI, Analysis of stretching of sheet metals with hemispherical punches. *Int. J. Mach. Tool Des.* **18**, 219–226 (1978).
57. E. D. PUGH, E. HINTON and O. C. ZIENKIEWICZ, A study of quadrilateral plate bending with reduced integration. *Int. J. Num. Meth. Engng* **12**, 1059–71 (1978).
58. O. C. ZIENKIEWICZ, R. L. TAYLOR and J. M. TOO, Reduced integration techniques in general analysis of plates and shells. *Int. J. Num. Meth. Engng* **3**, 275–290 (1971).

59. E. HINTON, E. M. SOLONEN and N. BICANIC, A study of locking phenomena in isoparametric elements. The Mathematics of Finite Elements. *Int. Conf. Brunel University*, 1978.
60. E. ONATE, E. HINTON and D. N. GLOVER, Techniques to improve the performance of Ahmad shell elements. *Proc. II Int. Conf. on Num. Modelling*, Madrid, 1978.
61. D. N. R. GLOVER, Examination of nine noded plate and curved shell elements with a hierarchical central node. M.Sc. Thesis. University College of Swansea, Swansea, 1978.
62. R. D. COOK, *Concepts and Applications of Finite Element Analysis*. Wiley, New York (1974).
63. T. J. R. HUGHES and M. COHEN, The 'Heterosis' finite elements for plate bending. *Comput. Structures* **9**, 445–450 (1978).

APPENDIX

The general visco-plastic constitutive relation

If elastic deformation is negligible, a very general description of behaviour of most materials can be given in terms of viscoplasticity. A particular form of this can be written following

Perzyna[47a] defines the strain rate $\dot{\epsilon}_{ij}$, by a general expression

$$\dot{\epsilon}_{ij} = \gamma\langle\phi(F)\rangle \frac{\partial Q}{\partial \sigma_{ij}} \tag{1a}$$

where

$$F = F(\sigma_{ij}, T, \epsilon_{ij}) \tag{2a}$$

is the description of a yield surface

$$Q = Q(\sigma_{ij}, T, \epsilon_{ij}) \tag{3a}$$

is a definition of a plastic potential.

Here

$$\begin{aligned} \langle\phi(F)\rangle &\equiv \phi(F) \quad \text{if } F \geqslant 0 \\ \langle\phi(F)\rangle &= 0 \qquad \text{if } F < 0 \end{aligned} \tag{4a}$$

and both the yield and potential functions may depend on temperature T. The particular form of the function ϕ can be defined to fit in with experimental data.

In general Q and F will be different specifying thus a non-associated flow but invariably the relationship (1) can be written in a form

$$\dot{\epsilon}_{ij} = \Gamma_{ijkl}\sigma_{kl} \tag{5a}$$

where

$$\Gamma = \Gamma(\sigma_{ij}, T, \epsilon_{ij})$$

is symmetric. Particular forms of above relationships are given explicitly in Ref. [47b] for several yield and potential surfaces.

The most common description of visco-plastic flow of metals (and many other materials) follows the assumption that both the yield and plastic potential surfaces are identified (i.e. the flow is associated) and that these depend only on the second stress strain invariant, i.e.

$$F = Q = \sqrt{3}\sqrt{J_2} - \sigma_y. \tag{6a}$$

Here

$$J_2 = \frac{1}{2} s_{ij} s_{ij}$$

is the second invariant of the deviatoric stress components s_{ij} and σ_y is the uniaxial yield stress.

In general σ_y itself is dependent on the temperatures T and the accumulated effective strain $\bar{\epsilon}$. This second invariant can be obtained by time integration of the appropriate rate expression given by

$$\dot{\bar{\epsilon}}^2_{ij} = 2\dot{\epsilon}_{ij}\dot{\epsilon}_{ij}/3. \tag{7a}$$

With Q written in terms of equation (6a) and assumed to be independent of strains and temperature we can write the general flow equation equivalent to equation (5a) as

$$\dot{\epsilon}_{ij} = \gamma\langle\phi(\sqrt{3}\sqrt{(J_2)} - \sigma_y)\rangle \frac{\sqrt{3}}{2\sqrt{J_2}} s_{ij} \tag{8a}$$

Clearly the strain rates implicit in above expression are such that

$$\dot{\epsilon}_{ij} = 0$$

i.e. the material flows without volume change and in the equivalent elastic model we have to assume incompressible behaviour.

We can compare the expression (8a) to a viscous isotropic shear deformation given by

$$\dot{\epsilon}_{ij} = \frac{1}{2\mu} s_{ij} \tag{9a}$$

in which μ is the viscosity coefficient. (In the elastic analogies the shear modulus is thus equivalent to viscosity).

The viscosity is identified using equation (8a) as

$$\frac{1}{2\mu} = \frac{\gamma\sqrt{3}}{2\sqrt{J_2}} \langle \phi(\sqrt{3}\sqrt{J_2} - \sigma_y) \rangle \tag{10a}$$

and this is a function of the stress level.

To write an equivalent expression in terms of the strain rate level we note from equation (9a) and (6a) that

$$J_2 = 2\mu^2 \dot{\epsilon}_{ij}\dot{\epsilon}_{ij} = (3\mu^2 \dot{\bar{\epsilon}}^2) \tag{11a}$$

Substituting above into equation (10a) we have

$$\dot{\bar{\epsilon}} = \gamma \quad (\phi(3\mu\dot{\bar{\epsilon}} - \sigma_y)) \tag{12a}$$

from which μ can be found for any strain rate function. A special but still quite general form of the function ϕ is an exponential type law and now equation (8a) takes the form

$$\dot{\epsilon}_{ij} = \gamma \langle (\sqrt{3}\sqrt{J_2} - \sigma_y)^n \rangle \frac{\sqrt{3}}{2\sqrt{J_2}} s_{ij}. \tag{13a}$$

In this case we can evaluate μ explicitly from equation (12a) as

$$\mu = \frac{\sigma_y + (\dot{\bar{\epsilon}}/\gamma)^{1/n}}{3\dot{\bar{\epsilon}}} \tag{14a}$$

Expressions (13a) and (14a) are widely applicable. Ideally plastic materials with a fixed yield point are simply obtained by taking $\gamma = \infty$ and give

$$\mu = \frac{\sigma_y}{3\dot{\bar{\epsilon}}}. \tag{15a}$$

This value tends to infinity as $\dot{\bar{\epsilon}}$ tends to zero so in numerical computation a large but finite cut off value must be assumed.

Such a cut off value defines in fact a finite viscosity everywhere thus allowing stresses to be computed even in zones where these are below the yield condition (rigid or nearly rigid behaviour). This model is used for most other subsequent computations.

A purely creeping material is characterised by $\sigma_y = 0$ and from equation (13a) we have in this case

$$\dot{\epsilon} = \frac{\gamma 3^{(n+1)/2}}{2} (\sqrt{J_2})^{n-1} s_{ij}. \tag{16}$$

This expression is identifiable with that used by Cornfield and Johnson[37] where, explicit temperature dependence is specified.

$$\dot{\epsilon}_{ij} = A(\sqrt{(J_2)^{n-1}} s'_{ij}\, e^{(-Q/RT)}). \tag{17}$$